Universitat Autònoma de Barcelona

Multifunctional Materials based on TTF-PTM dyads: towards new Molecular Switches, Conductors and Rectifiers

Manuel Souto Salom

Tesi doctoral

Programa de Doctorat en Ciència de Materials

Directors

Prof. Jaume Veciana i Dr. Imma Ratera

Departament de Química

Facultat de Ciències

2016

Chapter 3

NLO properties of TTF-π-PTM derivatives

3.1. Introduction

Nonlinear optics (NLO), the branch of optics which deals with the effect of the interaction of light with nonlinear media, has become an important research field during the last years due to its potential application in photoelectronics and photonics technology.[1–3] Indeed, this new technology, based on the acquisition and transfer of information by photons, shows many advantages such as higher speed of response and lower magnetic and electrical interactions during the processing of information. Thus, materials with nonlinear optical properties can be employed for the manipulation of optical signals in telecommunications as well as for other important technological applications such as optical computation, laser lithography and image processing.[4,5]

The first discovery of a nonlinear optical phenomenon was reported in 1961 when Franken and coworkers observed second harmonic generation (or frequency doubling) when they focused a ruby laser into a quartz crystal.[6] Since then the field of nonlinear optics became of high interest and many nonlinear optical effects and spectroscopic techniques were discover during the next decades.[7–11] Nonlinear optical activities were firstly found in semiconductors and inorganic crystals such as $LiNbO_3$. However, the commercial availability of such materials was limited since most of them exhibited low responses and were difficult to incorporate into microelectronic devices. During the decade of 1980 some organic materials were proposed as appropriate systems for obtaining high and efficient nonlinear responses since they are easier to integrate into optical devices.[12–14] Moreover, another advantage of the use of organic materials for NLO is the high versatility for designing new structures in order to establish relationships between structure-activity and control the nonlinear optical properties. However, organic compounds can show some disadvantages as the lack of transparency and optical stability due to damage when irradiated with high power light.

3.1.1. Theoretical aspects

NLO processes are the result of the interaction of intense electric fields with matter. When an electric field (E) of a laser beam is acting on a molecule, it induces electric polarization that produces a distortion in the spatial distribution between the electrons and nucleus since the propagation of the electromagnetic wave through the medium originates the vibration of electrons. The internal charge redistribution occurs in the opposite direction to the applied field and originates the appearance of induced dipoles, with moment μ. At very low fields, the induced polarization (p) is directly proportional to the intensity of the applied electric field and leads to Equation 1, in which μ_0 is the intrinsic dipole moment of the molecule and α is the linear polarizability of the molecule or atom. If the field oscillated with a frequency, then the induced polarization will have the same frequency and phase.

$$p = \mu_0 + \alpha \cdot E \qquad \text{(Eq. 1)}$$

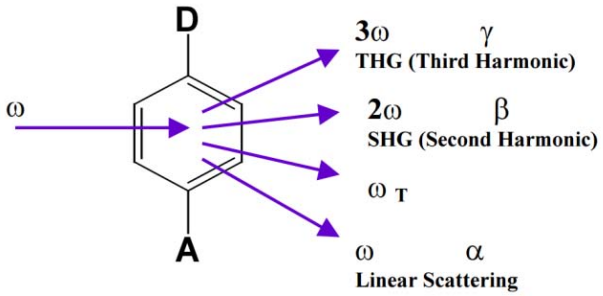

Figure 3.1. Linear and Nonlinear optical properties of a given material under high electric fields (*E*).

However, when a molecule is subject to a laser light (i.e. very intense electric field), the polarization becomes independent on the electric field and may change driving it beyond the linear regime (Figure 3.1). Therefore, the new nonlinear molecular polarization can be expressed by Equation 2, where α is the linear polarizability, β is the first hyperpolarizability (second-order effect) and γ is the second hyperpolarizability (third order effect) and so on.[15] Both coefficients are tensors and dependent on the direction of the incident wave with respect of the material orientation.

$$p = \mu_0 + \alpha \cdot E + \beta \cdot E \cdot E + \gamma \cdot E \cdot E \cdot E + \ldots \qquad \text{(Eq. 2)}$$

In general, to obtain materials with interesting NLO properties it is necessary to optimize the microscopic coefficient of the isolated molecules to the expression for the bulk polarization of a material when molecules are organized in crystals or in a condensed phase. In this case, macroscopic linear polarization is given by Equation 3, where P_0 is the static dipole of the sample, and $\chi^{(n)}$ is the nth order NLO susceptibility.

$$P = P_0 + \chi^{(1)} \cdot E + \chi^{(2)} \cdot E \cdot E + \chi^{(3)} \cdot E \cdot E \cdot E + \ldots \qquad \text{(Eq. 3)}$$

Some of the most common studied nonlinear optical phenomena are the second-harmonic generation (SHG) and the third-harmonic generation (THG). In SHG process (2ω:ω,ω) a beam with twice the optical frequency of the incoming one is generated (Figure 3.2). For example, by this process, near infrared laser light (ω) can be converted by a nonlinear optical material to blue light (2ω). It is important to mention that the used wavelengths of irradiation should not coincide with any important absorption region of the material to avoid resonant effects.

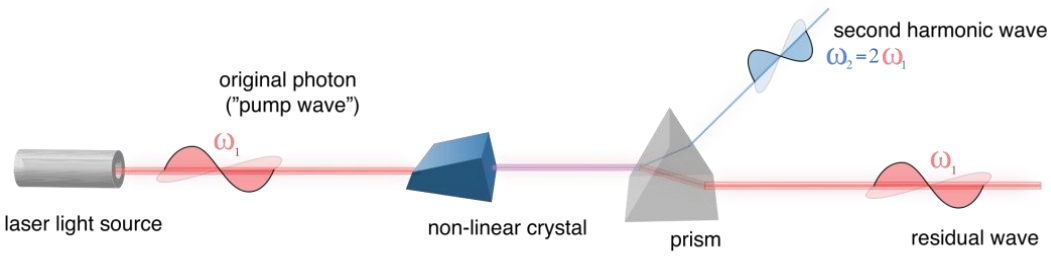

Figure 3.2. Scheme for SHG exhibting frequency doubling when a laser interacts on a crystal with NLO properties.

3.1.2. Experimental techniques

As we have seen, the nonlinear optical process (or hyperpolarizability of first order) consists on the frequency doubling of a laser when interacts with a material with nonlinear optical properties. The microscopic property is determined by β factor whereas the macroscopic property is defined by $\chi^{(2)}$ parameter. It is important to note that for β and $\chi^{(2)}$ to be non-zero, the molecules need to be non-centrosymmetric or to have a special symmetry like octupolar molecules. The main techniques for measuring the hyperpolarizability value β of isolated molecules in solution are Electric-Field-Induced Second Harmonic Generation (EFISHG) and Hyper-Rayleigh Scattering (HRS) techniques.

Electric-Field-Induced Second Harmonic Generation (EFISHG)

EFISGH technique has been used for many years since it was discovered by Terhune and coworkers in 1962.[16] The principle of this technique is based on the application of a static electric field that induces a preferential orientation of dipolar molecules dispersed in solution that will be aligned according to the direction of the field breaking the symmetry of the solution. Using the EFISHG technique it is possible to measure the product $\mu\beta_z$, where β_z is the z vectorial component of the β tensor (defining z as the direction of the permanent dipole moment). The disadvantage of EFISHG technique is that it involves the application of a strong electric field to break the centrosymmetry of the solution in order to orient the molecules. Thus, this approach can be applied only for non-ionic molecules which have a permanent dipole moment and it requires high concentrations, leading sometimes to the formation of undesired aggregates. Moreover, the measured quantity does not provide information about the value of β but just gives the $\mu\beta_z$ product. Because of these limitations the use of the EFISH technique is now quite limited.

Hyper-Rayleigh Scattering (HRS) techniques

Solutions are characterized by a disorder structure and exactly because of that they can produce incoherent harmonic light scattering, as predicted by Bersohn in 1964,[17] which allows to determine β values of several small organic molecules. In 1991, HRS was rediscovered as a valuable technique for measuring β values of organic chromophores by Clays and Perssons.[18,19] The Hyper-Rayleigh Scattering approach consists on a non-linear process where two photons at the fundamental frequency are converted into one photon at the second harmonic frequency. The two main advantages of HRS technique are that the hyperpolarizability β is determined independently of the dipole moment measuring the average in all directions and it can be applied to a wider range of compounds than EFISHG, such as ionic molecules in diluted solutions, or molecules with octupolar symmetry[20] (T or D_{3h}), such Crystal Violet.[21,22] An appropriate correction for multi-photon fluorescence is needed because the light is scattered in all directions and thus cannot be spatially separated from fluorescence. Pure solvent must be used as reference for the internal calibration of HRS measurements.

3.1.3. Organic materials for NLO

The capability of a material to find application for second-order NLO properties is determined by several factors such as the efficacy, the optical damage or the optical transparency. Traditionally, materials exhibiting second-order NLO responses were inorganic crystals, such as $LiNbO_3$, that show high optical transparency and optical damage resistance, but usually low β coefficients. However, organic materials, such as organic crystals and polymers, have been demonstrated to show better nonlinear optical and physical properties, such as ultrafast response times, lower dielectric constants or better processability characteristics, when compared to inorganic materials. Moreover, the ease of modification of organic molecular structures it makes possible to synthesize tailor-made molecules with desired physical properties.

3.1.4. *Push-pull* systems with NLO properties

Organic compound composed by an electron-donor fragment (D) linked to an electron-acceptor (A) through a π-conjugated spacer (know as *push-pull* systems) are one of the most developed structures for new compounds with efficient NLO responses. Indeed, as the theoretical Oudar and Chemla model suggests,[23] some of the requisites for obtaining molecules with large NLO responses are: a) excited electronic states close in energy to the ground state, b) large oscillator strengths for electronic transitions from the ground state and excited state, and c) a large difference between the ground (μ_g) and excited (μ_e) state dipole moments. Highly polarizable D-π-A dyads meet all these requierements showing charge transfer between the electron-donating and electron-withdrawing groups. For example, push-pull systems based on nitroaniline derivatives exhibit remarkable NLO properties (Figure 3.3).[24]

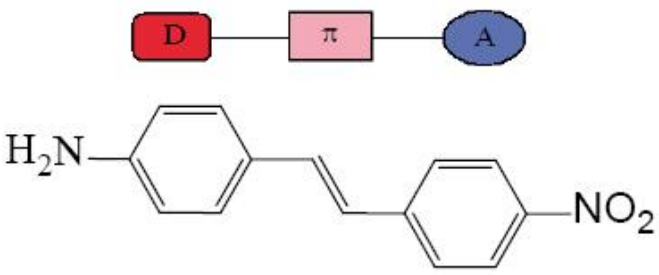

Figure 3.3. Molecular structure of the *push-pull* system 4-amino-4'-nitrostilbe.[24]

During the last years, high effort has been devoted to combine different bridges, acceptor and donor groups in several molecular systems in order to enhance its NLO response. Among the donor moieties, dimethylamino or alcoxibenzene units were extensively used groups whereas nitro, cyano and polycyano units were used as acceptor groups. Also the nature of the bridge was widely studied were polyenes, imines and aromatics systems were commonly used (Figure 3.4).

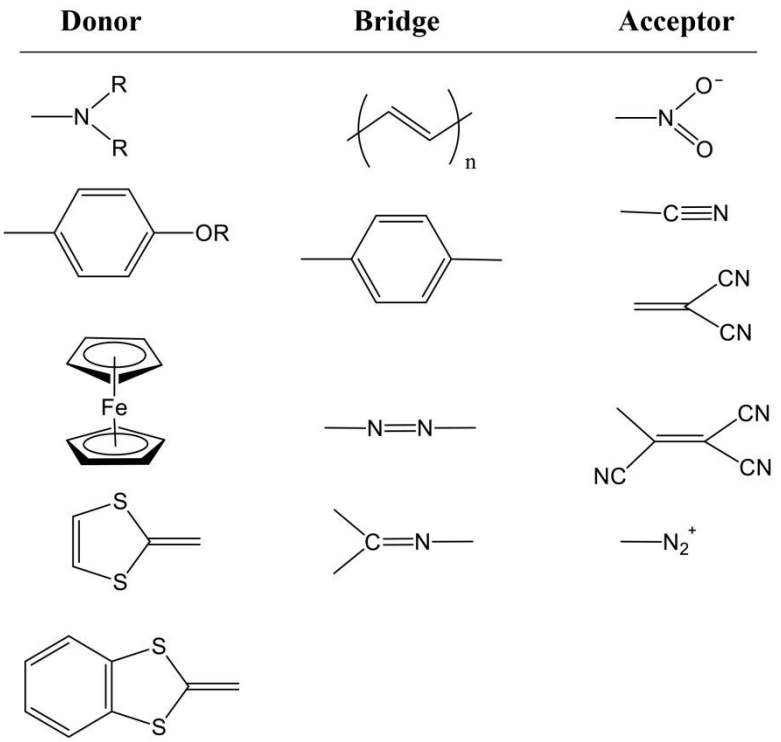

Figure 3.4. Most common units in *push-pull* molecules for second-order NLO properties.

The best theoretical description for explaining the second-order NLO phenomenon in dipolar conjugated molecules was established by Marder and coworkers[25,26] introducing the geometric parameter named BLA (Bond Length Alternation), which represents the average difference in length between adjacent C-C bonds in a polyene-like chain. This model provides a relationship between the β value and the degree of polarization of the molecules. For example, in substituted polyenes with weaker donor and acceptor units the neutral form dominates and the molecule shows a high degree of BLA; whereas stronger donor and acceptor groups can increase the contribution of the charge-separated resonant form and decrease the degree of bond length alternation. On the other hand, Prassad *et al.* studied the effect of conjugation of the bridge in 4-amino-β-nitroestirene derivatives showing that neither the increment of conjugation length nor the increment of the strength of the donor or acceptor units increase the NLO response due to the decreasing of the energy difference between the HOMO and LUMO transition.[27]

In principle, all efforts to increase the hyperpolarizability were centered on the search for stronger donor and acceptor units and the increasing of the π-conjugated bridge. In this sense, the first employed conjugated bridges were substituted benzenes, biphenyls, stilbenes or azostilbenes.[28] For example, the presence of a stronger donor and acceptor moieties connected through a longer bridge should give higher second-order NLO responses (Figure 3.5).[29] Thus, it is possible to obtain a large quantity of compounds modulating the degree of BLA by modifying the strength of the electroactive donor and acceptor units as well as the topology of the bridge.

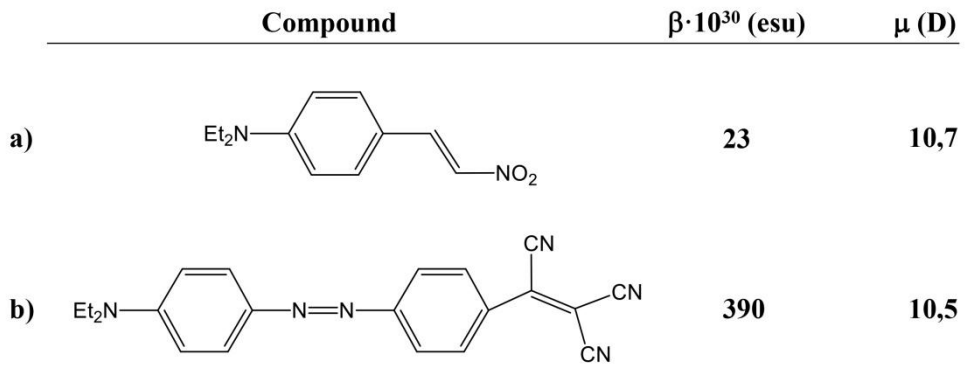

Figure 3.5. Hiperpolarizabilities (β) and permanent dipole moment (μ) of two conjugated *push-pull* compounds.[29]

TTF-based push-pull systems with NLO properties

Regarding electron-donor units for obtaining high NLO response, the tetrathiafulvalene (TTF) has been one of the most common used moieties due to its excellent donating properties and its enhanced aromaticity in the charged-separated state.[30] Some of these TTF-based push-pull compounds have been reported by Bryce, Orduna and Martín and are summarized in Figure 3.6.[31–36] The effect of increasing the length of the polyenic spacer and the influence of the nature of the acceptor moiety on the NLO properties was studied by using the EFISHG technique as well as by theoretical calculations. It was concluded that the nonlinear optical activity is larger for compounds containing better acceptor and $\mu\beta$ values increase with increasing the length of the ethylenic spacer.[34]

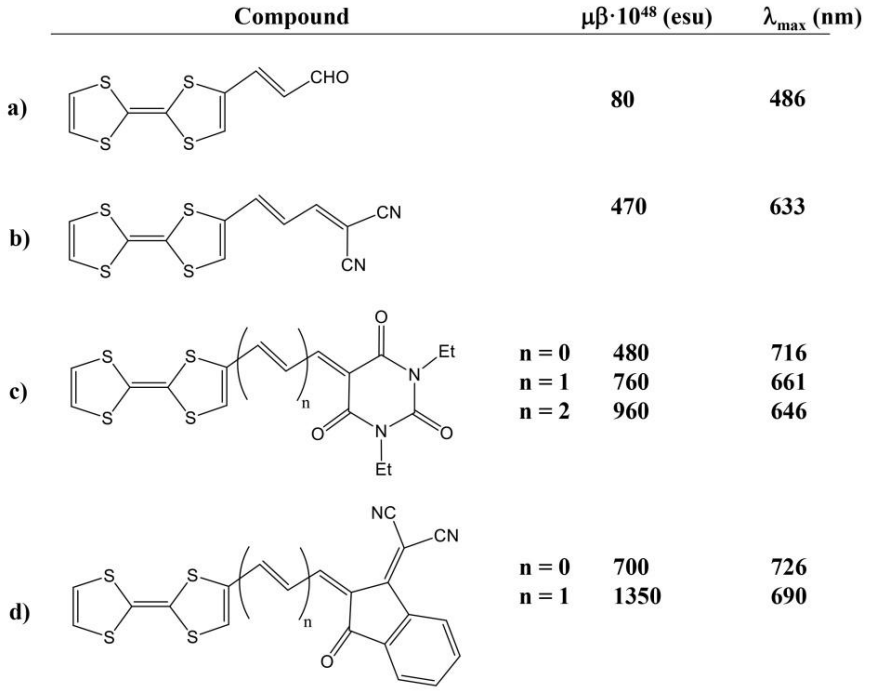

Figure 3.6. NLO properties and λ_{max} of TTF-based *push-pull* derivatives measured by EFIHG technique.[34]

Octupolar systems

In addition to the *push-pull* dipolar molecules, during the last decades there has been also a large interest for octupolar molecules exhibiting NLO responses as can afford advantages such as increased β responses without undesirable losses of transparency and improved phase-matching.[37,38] Octupolar molecules are non-dipolar species whose second-order NLO response is related to multidirectional charge transfer excitation, rather than to dipolar unidirectional excitations (Figure 3.7a). Indeed, the first hyperpolarizability cannot be described by the two-level model but is simplified into two components, $\beta_{J=3}$ (dipolar part) and $\beta_{J=1}$ (octupolar part). Due to the absence of dipole moment in such structures, it is not possible to measure the NLO responses in solution using EFISHG technique. Since the discovery of the HRS technique, which does not require a poling dipolar field, it has been possible to measure the NLO properties of octupolar systems. Most of the studied octupolar chromophores are based on trigonal organic (D_3 or D_{3h}) molecular systems such as triamino or trinitrobenzenes,[20,39] trisubstituted amines[40,41] or Crystal Violet derivatives[22] (Figure 3.7b). This later system has been extensively studied by Campo and Terenziani providing a detailed wavelength-dependent study of the molecular hyperpolarizability β of an octupolar NLO molecule for the first time.[21] Also bipyridyl ligands have demonstrated to be excellent building blocks for the construction of metal complexes like $[M(bpy)_3]^{n+}$ for which hyperpolarizability values are found to be between 200-500·10^{-30} esu (Figure 3.7c).[42–44]

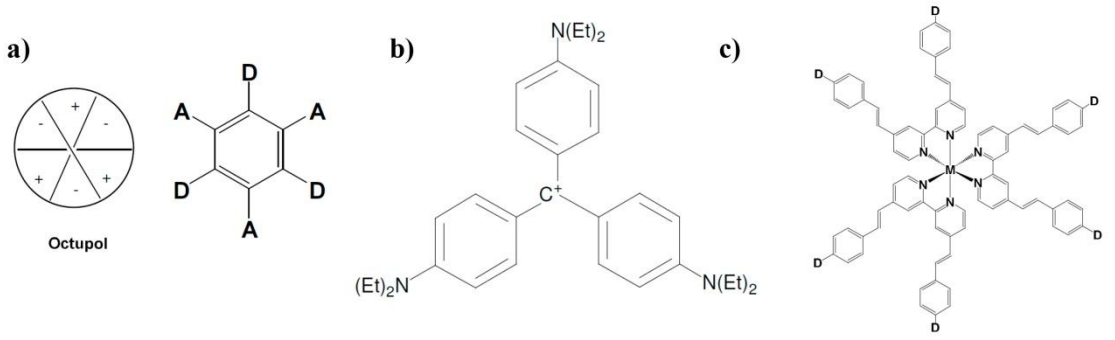

Figure 3.7. a) Octupolar charge distribution in a characteristic octupolar system and molecular structures of b) Crystal Violet and c) 4-4'-Dialkenyl-2-2'-bypiridines bearing π-donor substituents and its corresponding octahedral complexes.

3.1.4. Open-shell systems with NLO properties

During the last decades, most attempts to discover new molecular chromophores exhibiting large second-order hyperpolarizabilities were focused on closed-shell species. However, materials with open-shell structures have also aroused the interest of many researchers because their interesting second- and third-order NLO properties.[45,46] It was in 1996 when Di Bella *et al.* proposed that species having open-shell electronic states, as organic radical or transition metals with paramagnetic centers, can exhibit larger hyperpolarizabilities in comparison with analogous closed-shell systems.[47]

In fact, second-order NLO activities of systems with open-shell electronic states can be enhanced due to the more accessible charge-transfer electronic states. However, only few examples of organic open-shell molecules showing second-order hyperpolarizabilities have been reported due to the high chemical and thermal instability of these species. The first family of organic radicals whose NLO properties were attempted to be measured in solution was the α-nitronyl nitroxides,[48] but due to their low persistency they could not be studied in detail. Nicoud *et al.* reported the first organic radical based on the *p*-nitrophenyl α-nitronyl-nitroxide (NPNN) exhibiting both magnetic and nonlinear optical properties. The β hyperpolarizabilities were determined by the EFIGH technique obtaining a value of $6.24 \cdot 10^{-30}$ esu for NPNN.[49]

Triphenylmethyl-based systems with NLO properties

The capability of triphenylmethyl radical to generate NLO responses has been found to be higher due to the larger stability that allows to measure the corresponding hyperpolarizabilities using the HRS technique. In fact, molecular nonlinear optical coefficients of several polychlorotriphenylmethyl (PTM) radical derivatives, that show a non-planar D_3 symmetry group, were measured in CH_2Cl_2 solution at room temperature irradiating with a laser light at 1064 nm (Figure 3.8).[50,51] Interestingly, high NLO responses with larger β values ($118\text{-}775 \cdot 10^{-30}$ esu) were obtained being up to five times larger than the one reported for the closed-shell Crystal Violet compound ($150 \cdot 10^{-30}$ esu) that exhibits a similar $Ar^1Ar^2Ar^3Z$ topology. Moreover, the representation of the hyperpolarizabilities β in front of the reduction or oxidation potentials of the radicals gave a linear dependence indicating a direct correlation between the energy of the electronic transitions (where the SOMO orbital is involved) and the NLO responses.

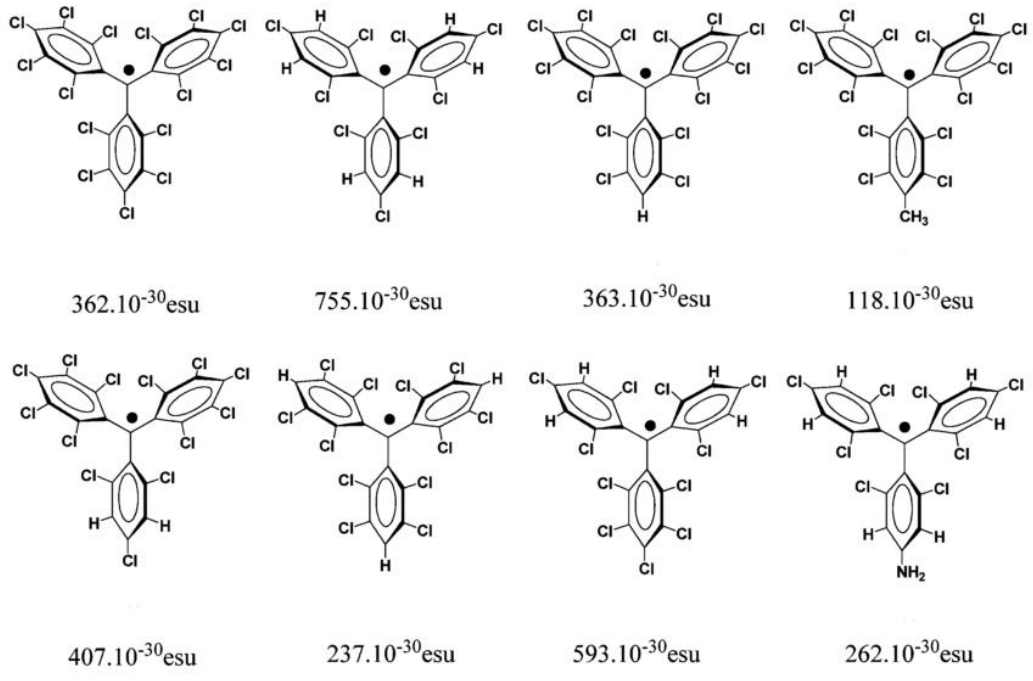

Figure 3.8. Hyperpolarizability β values of several PTM radicals measured with the HRS technique.

The incorporation of PTM radicals into push-pull systems has been shown to be very efficient to develop new molecular systems with large NLO responses. On the other hand, the incorporation of metallocene moieties as donor groups linked to acceptor moieties has been widely studied since the discovery of large second-order NLO properties in a ferrocene (Fc) derivative reported by Green and coworkers.[52] In this direction, it has been reported some *push-pull* systems based on the electron-acceptor PTM radical linked to the electron-donor Fc moiety through a vinylene bridge. For example, NLO properties measured by EFISHG technique of the isomeric *trans* and *cis* forms of Fc-PTM dyad revealed that molecular torsions decreased the second-order NLO response (Figure 3.9).[53]

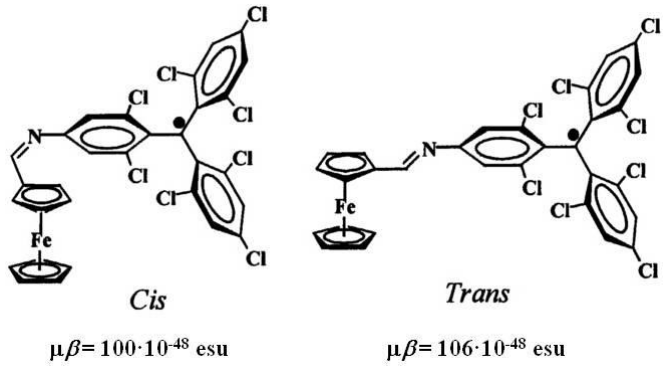

Figure 3.9. Vectorial hyperpolarizability $\mu\beta$ values of the two isomers (*cis*- and *trans*-) of the Fc-PTM radical dyad measured with the EFISHG technique

Moreover, NLO properties of the push-pull system based on the PTM radical linked to the nonamethylferrocene group by a vinylene bridge (Me_9Fc-PTM) were investigated using HRS technique with a laser of 800 nm (Figure 3.10).[54] The Fc-PTM radical dyad gave a NLO response with a dynamic hyperpolarizability value β of $545 \cdot 10^{-30}$ esu. Interestingly, this value was reduced to $66 \cdot 10^{-30}$ esu for the corresponding Me_9Fc^+-PTM cation and even more for the related carbanion Me_9Fc-PTM$^-$ ($30 \cdot 10^{-30}$ esu).

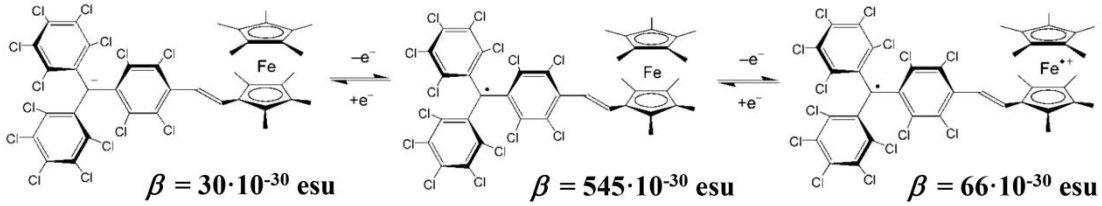

Figure 3.10. The hyperpolarizability β values for the three redox states of Me_9Fc-PTM dyad.

3.2. Results and discussion

In view of the donors and acceptor capabilities and large NLO properties of both TTF and PTM radical molecules, it could be very interesting to combine both units in a D-π-A molecule and evaluate its second-order NLO response. For this reason and in order to evaluate the influence of the open-shell character and the length of the bridge, we have synthesized and characterized a family of TTF-π-PTM radical derivatives (**1, 3** and **4**) and their non-radical analogues (**1-H**, **3-H** and **4-H**) increasing the number of vinylene units between the D and A units (see Publication #3).

3.2.1. NLO properties of TTF-π-PTM dyads

In this Chapter we provide a detailed study of the intramolecular charge transfer dependence on the open-shell structure and on the bridge length of this family of compounds (Figure 3.11). Moreover, NLO properties of such dyads have been evaluated by means of the Hyper-Rayleigh Scattering (HRS) technique. HRS measurements have been performed, in collaboration with V. Pia and W. Wenseelers (University of Antwerp), using a wavelength of 1550 nm that show a direct correlation between the open-shell character of the dyads and the bridge length with the β hyperpolarizabilities. Moreover, theoretical calculations, made by E. Ortí and coworkers (ICMol, Universidad de Valencia), have been carried out in order to further understand the electronic, geometrical and NLO properties of these TTF-π-PTM dyads.

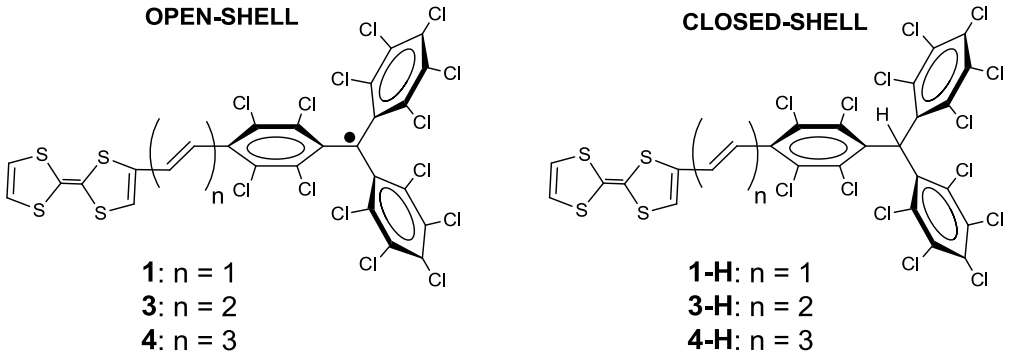

Figure 3.11. Molecular structures of the radical dyads **1, 3** and **4** and their non-radical derivatives **1-H**, **3-H** and **4-H**.

Cyclic voltammetry of radicals **1, 3** and **4**, as well as their non-radical precursors **1-H**, **3-H** and **4-H**, were performed in CH_2Cl_2 at room temperature (Table 1 and Figure 3.12). As expected the CV of radical dyads exhibits three waves, related to the following redox pairs: $PTM^-/PTM\bullet$, $TTF/TTF^{+}\bullet$, and $TTF^{+}\bullet/TTF^{2+}$. It is important to note that the oxidation waves assigned to the TTF moiety are higher than the unsubstituted TTF in agreement with the presence of an acceptor moiety. Moreover, these peaks shifted toward more positive values as the length of the spacer decreases, from **4** to **1**, indicating a stronger interaction between the donor and acceptor moieties when are closer.

Table 1. Cyclic voltammetries data of compounds **1**, **3** and **4** in CH_2Cl_2, vs. Ag/AgCl, using *n*-Bu_4PF_6 (0.1 M) as electrolyte at 300 K under argon at a scan rate of 0.1 V/s.

Compound	$E^{red}_{1/2}$ (V)	$E^{ox1}_{1/2}$ (V)	$E^{ox2}_{1/2}$ (V)	ΔE_{red}(V)[a]	ΔE_{ox}(V)[b]
1	-0.16	0.50	1.01	0.66	0.51
3	-0.20	0.44	0.96	0.64	0.52
4	-0.22	0.40	0.92	0.62	0.52

a) $\Delta E_{red} = E^{ox1}_{1/2} - E^{red}_{1/2}$; b) $\Delta E_{ox} = E^{ox2}_{1/2} - E^{ox1}_{1/2}$.

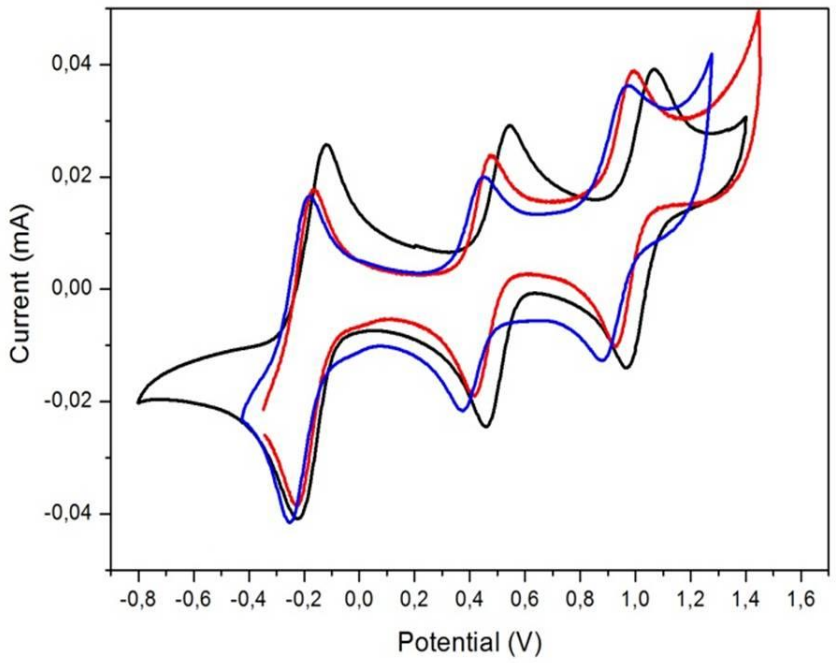

Figure 3.12. Cyclic voltammetry of solutions of radical compounds **1** (black line), **3** (red line) and **4** (blue line) in CH_2Cl_2, vs. Ag/AgCl, using *n*-Bu_4PF_6 (0.1 M) as electrolyte at 300 K under argon at a scan rate of 0.1 V/s.

On the other hand, UV-vis-NIR spectra of all compounds were measured in CH_2Cl_2 at 300 K. We calculated the HOMO-LUMO or HOMO-SUMO gaps from the lowest energy band observing considerable large gaps for the closed-shell dyads (~2 eV) whereas these are smaller for the open-shell dyads (Table 2). It is important to mention that there is no direct correlation between the electrochemical and optical gaps, which hinders determination of HOMO-LUMO gaps as it has been already observed for similar systems.[34] This fact can be attributed to the irreversible nature of the electrochemical reduction, where the peak potential does not correspond to the thermodynamic redox potential. In these similar cases, the elongation of the π-linker between the donor and acceptor results in small but consistent hypsochromic shifts of the long-wavelength absorption, although the electrochemical gap is reduced. Regardless of this behavior, the hyperpolarizability of similar TTF-π–A compounds increases with elongation of the π-linker (See Figure 3.6).[55] On the other hand, DFT calculations have been performed in order to assign each band and to calculate the HOMO-LUMO gap observing the same trend that in the experimental one.

Table 2. UV-vis-NIR data for compounds **1, 3**, **4** and **1-H**, **3-H**, **4-H** (lowest energy bands in bold) in CH_2Cl_2. Experimental and theoretical HOMO-LUMO gaps calculated from the spectra.

Compound	λ_{max}/nm ($10^{-3}\varepsilon/M^{-1}\,cm^{-1}$)	exp HOMO-LUMO gap (eV)	theo HOMO-LUMO gap (eV)
1	295 (20.6); 323 (sh); 385 (26); 426 (15); 518 (4.3); **957** (0.6)	0.96	1.13
3	273 (sh); 326 (21.8); 385 (29.3); 456 (12.3); 568 (4.5); **942** (0.6)	1.00	1.09
4	340 (24.9); 385 (30.1); 475 (15.9); 607 (7.4); **918** (0.7)	1.05	1.07
1-H	290 (sh); 322 (28.4); **456** (5.4)	2.20	2.65
3-H	289 (sh); 332 (26.4); **463** (5.4)	2.15	2.45
4-H	278 (sh); 355 (24.8); **471** (6.4)	2.10	2.31

UV-Vis-NIR spectra of radical dyads **1**, **3** and **4** show an intense band at 386 nm that is characteristic of PTM radical chromophores (Figure 3.13). Two unresolved peaks appear at lower energies (426, 456 and 475 nm, and 518, 568 and 607 nm for **1**, **3** and **4** respectively) which are attributed to the electronic conjugation of the unpaired electron into the π-framework. The tendency of these bands is to shift toward lower energies when increasing the bridge length in agreement with the higher electron delocalization over the vinylene units. Finally, we can observe the appearance of a weak broad band between 900-1100 nm that is assigned to an ICT process from the TTF unit to the PTM radical. This band is shifted toward higher energies when increasing the length of oligoenic bridge in agreement with the reduced charge transfer between the donor and the acceptor.

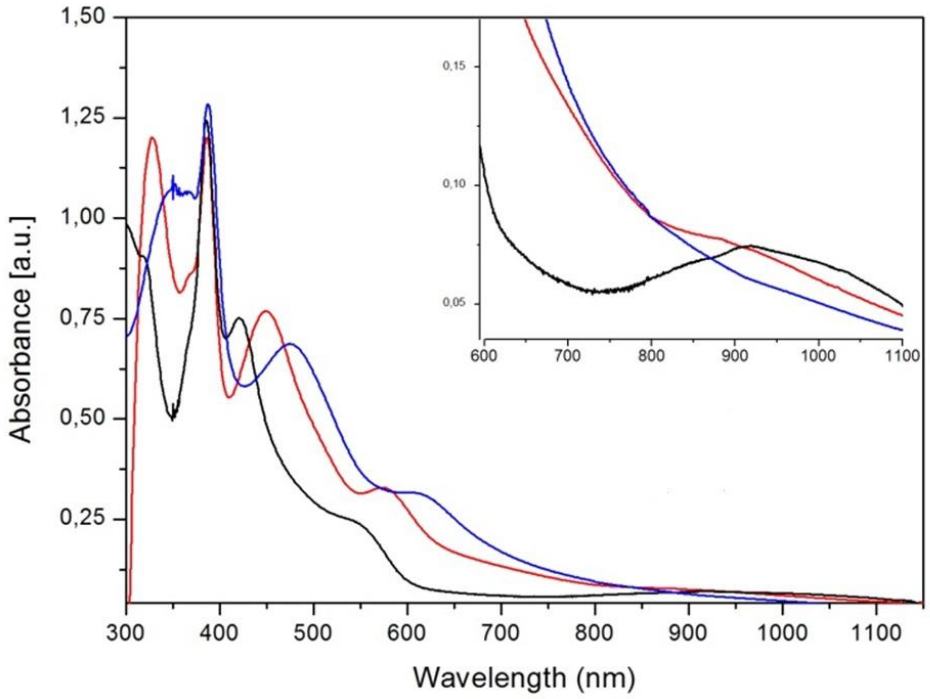

Figure 3.13. UV-vis-NIR spectra of a solution 0.05 mM of dyads **1** (black line), **3** (red line) and **4** (blue line) in CH_2Cl_2. Inset shows the low-energy range of the absorption spectra.

Moreover, vibrational spectroscopy gave us further information about the degree of ICT of these *push-pull* chromophores. The Raman spectra of dyads **1**, **3** and **4** were recorded at 300 K by using an excitation wavelength of λ=514 nm. Raman lines around 1600 cm^{-1} can be attributed to a ν(C=C) stretching mode of the vinylenic spacer, bands between 1570-1550 cm^{-1} are due to ν_s(C=C) stretching (ν_4 mode) of the TTF donor unit,[34] whereas the line around 1520-1500 cm^{-1} are characteristic for the stretching mode of the lateral polychlorinated benzene groups overlapped with the *n*(C=C) stretching vibration of the TTF group. The band related to the external spin bearing PTM moiety is reported at 1509 cm^{-1} for the PTM radical without substituents and shifts towards higher frequencies when PTM radical exerts a more profound electron withdrawal over a richer electron donor unit.[56] In this case, we can observe that this band is shifted from 1516 to 1508 cm^{-1} for **1** and **4**, respectively (Figure 3.14), in agreement with the higher degree of charge transfer from the TTF electron donor to the PTM radical acceptor unit when the bridge becomes shorter. Moreover, the band related to the TTF group is upshifted when increasing the length of the π-bridge (from 1552 to 1569 cm-1 for **1** and **4**, respectively) indicating a higher degree of the charge transfer in the TTF unit for the shortest dyad **1** as it has been already observed for similar TTF derivatives.[34] This fact is in agreement with the calculated Mulliken charges showing that the TTF unit donates more electron density as the bridge becomes shorter.

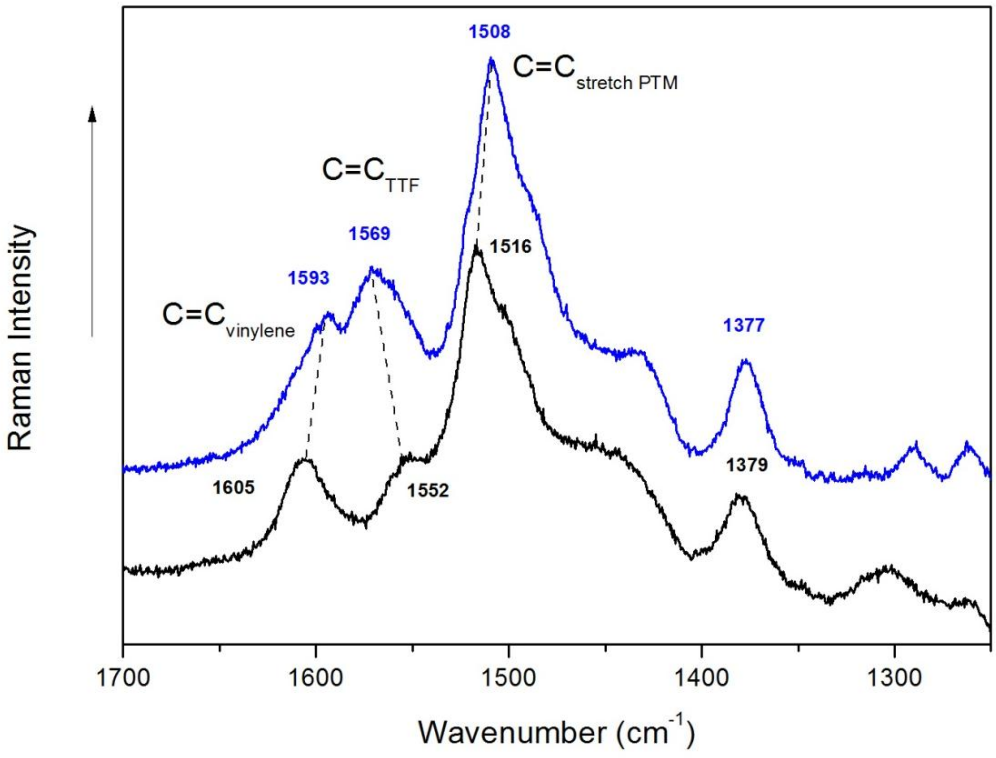

Figure 3.14. Raman spectra of compounds **1** (black line) and **4** (blue line)

Finally, in order to evaluate the NLO properties of open-shell **1**, **3** and **4** dyads and closed-shell **1-H**, **3-H** and **4-H** dyads, we have performed HRS measurements in collaboration with W. Wenseelers during a research stay at the University of Antwerp. Molecular nonlinear coefficients β of these compounds **1**, **3**, **4** and **1-H**, **3-H**, **4-H** were determined in $CHCl_3$ solution at room temperature using HRS experiments with a wavelength of 1550 nm. A worth noticing point of the experimental values is the large increase of β values of radical compounds in comparison with the non-radical ones that ranges from 2.5 to 10 times. Moreover, there is an increase of the hyperpolarizability when the bridge length is enlarged in accordance with the enhancement of the electronic delocalization (Table 3 and Figure 3.15). Theoretical calculations of NLO properties made by E. Ortí and coworkers confirmed the observed tendency when increasing the conjugated bridge as well as when comparing the non-radical and radical compounds.

Table 3. Experimental and theoretical NLO properties of **1**, **3**, **4**, **1-H**, **3-H** and **4-H** compounds using a laser of λ = 1550 nm.

Compound	exp β (10^{-30}esu) [a]	theo β (10^{-30}esu) (B3LYP/6-31G**)
1	440	2500
3	600	3500
4	880	4500
1-H	49	10
3-H	90	250
4-H	175	510

[a] Measured in $CHCl_3$ at λ = 1550 nm.

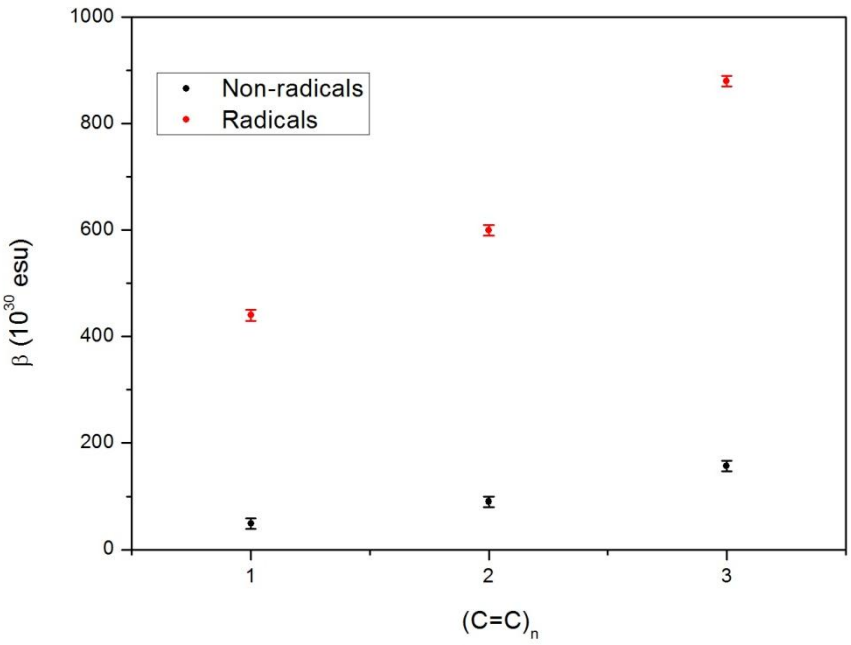

Figure 3.15. Representation of hyperpolarizabilities β for the radical and non-radical dyads with different number of vinylenic units measured at λ = 1550 nm.

3.3. Summary

In summary, we have reported the synthesis and physiochemical properties of a new family of TTF-π-PTM derivatives of three conjugated donor-π-acceptor radical systems (**1**, **3** and **4**) based on a tetrathiafulvalene (TTF) unit, as electron-donor, connected to a polychlorotriphenylmethyl (PTM) radical, as electron-acceptor, through different ethylenic units as bridge, exhibiting large nonlinear optical properties. These results are detailed in Publication #3.

The bridge length dependence on the intramolecular charge transfer has been analyzed by different electrochemical and spectroscopic techniques, such as CV, UV-vis-NIR, IR, Raman, and ESR. In addition, the second-order non-linear optical (NLO) response of these derivatives have been studied using the HRS technique demonstrating a direct dependence on the bridge length as well on the open-shell structure comparing with their non-radical analogues (**1-H**, **3-H** and **4-H**). Interestingly, an enhanced NLO response was observed when the PTM is in its radical form as well as the length of the bridge becomes larger. Indeed, the NLO β hyperpolarizabilities of radical compounds in comparison with the non-radical ones that ranges from 2.5 to 10 times. Moreover, theoretical calculations supported all the electronic, geometrical and NLO properties of such TTF-π-PTM dyads. In conclusion, these conjugated TTF-π-PTM compounds have demonstrated to be very promising for the development of new materials exhibiting large NLO responses that can be enhanced increasing the conjugation of the systems. These results could open new possibilities to design new multifunctional and/or switchable materials exhibiting simultaneously magnetism and NLO properties.

3.4. References

1. Boyd, R. W. *Nonlinear Optics*. (Academic Press, Inc., 1992).

2. Zyss, J. *Molecular Nonlinear Optics*. (Academic Press, Inc., 1993).

3. Zyss, J. *Nonlinear Optics: Materials, Physics and Devices*. (Academic Press, Inc., 1993).

4. Marder, S. R., Kippelen, B., Jen, A. K.-Y. & Peyghambarian, N. Design and synthesis of chromophores and polymers for electro-optic and photorefractive applications. *Nature* **388,** 845–851 (1997).

5. Long, N. J. Organometallic Compounds for Nonlinear Optics-The. *Angew. Chemie - Int. Ed.* **34,** 21–38 (1995).

6. Franken, P. A., Hill, A. E., Peters, C. W. & Weinreich, G. Generation of Optical Harmonics. *Phys. Rev. Lett.* **7,** 118–120 (1961).

7. Burland, D. Optical Nonlinearities in Chemistry: Introduction. *Chem. Rev.* **94,** 1–2 (1994).

8. Williams, D. J. Organic Polymeric and Non-Polymeric Materials with Large Optical Nonlinearities. *Angew. Chemie - Int. Ed.* **23,** 690–703 (1984).

9. Marder, S. R. & Perry, J. W. Molecular Materials for Second-Order Nonlinear Optical Applications. *Adv. Mater.* **5,** 804–815 (1993).

10. Nie, W. Optical Nonlinearity : Phenomena , Applications , and Materials. *Adv. Mater.* **5,** 520–545 (1993).

11. Kanis, D. R., Ratner, M. A. & Marks, T. J. Design and Construction of Molecular Assemblies with Large Second-Order Optical Nonlinearities. Quantum Chemical Aspects. *Chem. Rev.* **94,** 195–242 (1994).

12. Chemla, D. S. & Zyss, J. *Nonlinear Optical Properties of Organic Molecules and Crystals*. (Academic Press, Inc., 1987).

13. Williams, D. J. *Nonlinear Optical Properties of Organic and Polymeric Materials*. (American Chemical Society, 1983).

14. Marks, T. J. & Ratner, M. A. Design, Synthesis, and Properties of Molecule-Based Assemblies with Large Second-Order Optical Nonlinearities. *Angew. Chem. Int. Ed. Engl.* **34,** 155–173 (1995).

15. Prassad, N. O. & Williams, D. J. *Introduction to Nonlinear Optical Effects in Molecules and Polymers*. (Wiley-Interscience, 1991).

16. Terhune, R. W., Maker, P. D. & Savage, C. M. Optical Harmonic Generation in Calcite. *Phys. Rev. Lett.* **8,** 404–406 (1962).

17. Bersohn, R. Scattering of Optical Harmonics by Macromolecules. *J. Am. Chem. Soc.* **86,** 3505–3507 (1964).

18. Clays, K. & Persoons, A. Hyper-Rayleigh Scattering in Solution. *Phys. Rev. Lett.* **66,** 2980–2983 (1991).

19. Clays, K. & Persoons, A. Hyper Rayleigh scattering in solution. *Rev. Sci. Instrum.* 3285–3289 (1992).

20. Verbiest, T., Clays, K., Samyn, C., Reinhoudt, J. W. D. & Persoonst, A. Investigations of the Hyperpolarizability in Organic Molecules from Dipolar to Octopolar Systems. *J. Am. Chem. Soc.* **116,** 9320–9323 (1994).

21. Campo, J. *et al.* First Hyperpolarizability Dispersion of the Octupolar Molecule Crystal Violet : Multiple Resonances and Vibrational and Solvation Effects. *J. Am. Chem. Soc.* **132**, 16467–16478 (2010).

22. Chui, T. W. & Wong, K. Y. Study of hyper-Rayleigh scattering and two-photon absorption induced fluorescence from crystal violet. *J. Chem. Phys.* **109**, 1391–1396 (1998).

23. Oudar, J. L. & Chemla, D. S. Hyperpolarizabilities of the nitroanilines and their relations to the excited state dipole moment. *J. Chem. Phys.* **66,** 2664–2668 (1977).

24. Lamèrere, J. F. *et al.* Synthesis, characterization and nonlinear optical (NLO) properties of a push – pull bisboronate chromophore with a potential electric field induced NLO switch. *J. Mater. Chem.* **16,** 2913–2920 (2006).

25. Marder, S. R., Beratan, D. N. & Cheng, L.-T. Approaches for Optimizing the First Electronic Hyperpolarizability of Conjugated Organic Molecules. *Science* **252,** 103–106 (1991).

26. Marder, S. R. *et al.* Direct Observation of Reduced Bond Length Alternation in Donor / Acceptor Polyenes. *J. Am. Chem. Soc.* **115,** 2524–2526 (1993).

27. Keshari, V., Karna, S. P. & Prasad, P. N. Ab Initio Time-Dependent Coupled Perturbed Hartree-Fock Studies of Optical Nonlinearities of Organic Molecules : Alkyl Derivatives of 4-Amino-nitrostyrene. *J. Phys. Chem.* **97,** 3525–3529 (1993).

28. Katz, H. E. *et al.* Greatly Enhanced Second-Order Nonlinear Optical Susceptibilities in Donor-Acceptor Organic Molecules. *J. Am. Chem. Soc.* **109,** 6561–6563 (1987).

29. Marder, S. R. *et al.* Large First Hyperpolarizabilities in Push-Pull Polyenes by Tuning of the Bond Length Alternation and Aromaticity. *Science* **263,** 511–514 (1994).

30. Segura, J. L. & Martín, N. New concepts in tetrathiafulvalene chemistry. *Angew. Chemie - Int. Ed.* **40,** 1372–1409 (2001).

31. De Lucas, A. I. *et al.* The first tetrathiafulvalene derivatives exhibiting second-order NLO properties. *Tetrahedron* **54,** 4655–4662 (1998).

32. Moore, A. J. *et al.* Synthesis , Structures and Nonlinear Optical Properties of Novel D-π-A Chromophores : Intramolecular Charge Transfer from 1, 3-Dithiole or Ferrocene Moieties to Polynitrofluorene or Dicyanomethylene Moieties through Conjugated Linkers. *Eur. J. Org. Chem.* 2671–2687 (2001).

33. Bryce, M. R. *et al.* Synthesis of Conjugated Tetrathiafulvalene (TTF)-π-Acceptor Molecules Intramolecular Charge Transfer and Nonlinear Optical Properties. *Eur. J. Org. Chem.* 1927–1935 (2001).

34. González, M. *et al.* Tetrathiafulvalene Derivatives as NLO-phores : Synthesis, Electrochemistry, Raman Spectroscopy, Theoretical Calculations, and NLO Properties of Novel TTF-Derived Donor-π-Acceptor Dyads. *J. Org. Chem.* **66,** 8872–8882 (2001).

35. Alías, S. *et al.* Synthesis, Structure, and Optical Properties of 1,4-Dithiafulvene-Based Nonlinear Optic-phores. *J. Org. Chem.* **72,** 6440–6446 (2007).

36. Alías, S. *et al.* Iminium salts of ω-dithiafulvenylpolyenals: An easy entry to the corresponding aldehydes and doubly proaromatic nonlinear optic-phores. *J. Org. Chem.* **73,** 5890–5898 (2008).

37. Zyss, J. & Ledoux, I. Nonlinear Optics in Multipolar Media : Theory and Experiments. *Chem. Rev.* **94,** 77–105 (1994).

38. Kim, H. M. & Cho, B. R. Second-order nonlinear optical properties of octupolar molecules structure – property relationship. *J. Mater. Chem.* **19,** 7402–7409 (2009).

39. Ledoux, I., Zyss, J., Siegel, J. S., Brienne, J. & Lehn, J.-M. Second-harmonic generation from non-dipolar non-centrosymmetric aromatic charge-transfer molecules. *Chem Phys Lett* **172,** 440–444 (1990).

40. Stadler, S., Braüchle, C., Brandl, S. & Gompper, R. Experimental Determination of the First Hyperpolarizability of New Chiral and Achiral Octupolar Tertiary Amines by Hyper-Rayleigh Scattering. *Chem. Mater.* **8,** 414–417 (1996).

41. Argouarch, G. *et al.* Donor-substituted triaryl-1,3,5-triazinanes-2,4,6-triones: octupolar NLO-phores with a remarkable transparency–nonlinearity trade-off. *New. J. Chem* **35,** 2409–2411 (2011).

42. Maury, O. & Bozec, H. L. E. Molecular Engineering of Octupolar NLO Molecules and Materials Based on Bipyridyl Metal Complexes. *Acc. Chem. Res.* **38,** 691–704 (2005).

43. Feuvrie, C. *et al.* Nonlinear Optical and Two-Photon Absorption Properties of Octupolar Tris (bipyridyl) metal Complexes. *J. Phys. Chem. A* **111,** 8980–8985 (2007).

44. Vance, F. W. & Hupp, J. T. Probing the Symmetry of the Nonlinear Optic Chromophore Ru(trans-4,4′-diethylaminostyryl-2,2′-bipyridine)$_3^{2+}$: Insight from Polarized Hyper-Rayleigh Scattering and Electroabsorption (Stark) Spectroscopy. *J. Am. Chem. Soc.* **121,** 4047–4053 (1999).

45. Nakano, M. & Champagne, B. Nonlinear optical properties in open-shell molecular systems. *Comput Mol Sci* **6,** 198–210 (2016).

46. Nakano, M. & Fukuda, K. Third-Order Nonlinear Optical Properties of Asymmetric Non-Alternant Open-Shell Condensed-Ring Hydrocarbons : Effects of Diradical Character, Asymmetricity, and Exchange Interaction. *J. Phys. Chem. C* **120,** 1193–1207 (2016).

47. Di Bella, S., Fragalà, I., Marks, T. J. & Ratner, M. A. Large second-order optical nonlinearities in open-shell chromophores. Planar metal complexes and organic radical ion aggregates. *J. Am. Chem. Soc.* **118,** 12747–12751 (1996).

48. Angeloni, L. *et al.* Crystal Structures, Magnetic and Non-linear Optical Properties of methoxiphenyl nitronyl-nitroxide radicals. *J. Mater. Chem.* **4,** 1047–1053 (1994).

49. Nicoud, J.-F., Serbutoviez, C., Puccetti, G., Ledoux, I. & Zyss, J. Hyperpolarizability of new nitro-aromatic-N-oxide species: nonlinear optical properties of a ferromagnetic organic material. *Chem. Phys. Lett.* **175,** 257–261 (1990).

50. Ratera, I. *et al.* Nonlinear optical properties of open-shell polychlorotriphenylmethyl radicals. *Polyhedron* **22,** 1851–1856 (2003).

51. Ratera, I. *et al.* Nonlinear optical properties of polychlorotriphenylmethyl radicals: Towards the design of 'super-octupolar' molecules. *Chem. Phys. Lett.* **363,** 245–251 (2002).

52. Green, M. L. H. *et al.* Synthesis and structure of (cis)-[1-ferrocenyl-2-(4-nitrophenyl)ethylene], an organotransition metal compound with a large second-order optical nonlinearity. *Nature* **330,** 360–362 (1987).

53. Ratera, I. *et al.* Nonlinear optical properties of a new stable ferrocenyl Schiff-base polychlorotriphenylmethyl radical. *Synth. Met.* **121,** 1834–1835 (2001).

54. Sporer, C. *et al.* A Molecular multiproperty switching array based on the redox behavior of a ferrocenyl polychlorotriphenylmethyl radical. *Angew. Chemie - Int. Ed.* **43,** 5266–5268 (2004).

55. Bendikov, M., Wudl, F. & Perepichka, D. F. Tetrathiafulvalenes, oligoacenenes, and their buckminsterfullerene derivatives: The brick and mortar of organic electronics. *Chem. Rev.* **104,** 4891–4946 (2004).

56. González, S. R. *et al.* Diradicals acting through diamagnetic phenylene vinylene bridges: Raman spectroscopy as a probe to characterize spin delocalization. *J. Chem. Phys.* **140,** 164903 (2014).

Publication #3

Title: Non-Linear Optical Properties of Push-pull TTF-π-PTM Radicals: the Role of the Open-Shell Structure and Bridge Length

Authors: Manuel Souto, Valentina Pia, Imma Ratera, Enrique Ortí, Wim Wenseelers, and Jaume Veciana

Publication: *In preparation*

Non-Linear Optical Properties of Push-pull TTF-π-PTM Radicals: the Role of the Open-Shell Structure and Bridge Length

Manuel Souto,[†] Valentina Pia,[‡] Imma Ratera,[†] Enrique Ortí,[⊥] Wim Wenseelers,[‡] and Jaume Veciana[†,*]

[†] Institut de Ciència de Materials de Barcelona (ICMAB-CSIC)/CIBER-BBN, Campus Universitari de UAB, 08193 Cerdanyola del Vallès (Barcelona), Spain

[⊥] Instituto de Ciencia Molecular, Universidad de Valencia, 46980 Paterna, Spain

[‡] Department of Physics, University of Antwerp (campus Drie Eiken), Universiteitsplein 1, B-2610 Wilrijk-Antwerpen, Belgium

ABSTRACT: In this article, a family of three conjugated donor-π-acceptor radical systems (**1a-1c**) based on a tetrathiafulvalene (TTF) unit, as electron-donor, connected to a polychlorotriphenylmethyl (PTM) radical, as electron-acceptor, through different ethylenic units as bridge has been synthesized. The bridge length dependence on the intramolecular charge transfer has been analyzed by different electrochemical and spectroscopic techniques, such as CV, UV-vis-NIR, IR, Raman, and ESR. In addition, the second-order non-linear optical (NLO) of these derivatives have been studied using the HRS technique demonstrating a direct dependence on the bridge length as well on the open-shell structure comparing with their non-radical analogues (**2a-2c**). Interestingly, an enhanced NLO response was observed when the PTM is in its radical form as well as the length of the bridge becomes larger.
SECTION: Donor-acceptor, push-pull, tetrathiafulvalene, PTM radical, intramolecular charge-transfer, NLO properties.

The design and synthesis of novel organic materials exhibiting nonlinear optical (NLO) properties is an interesting field due to their potential applications in optoelectronic technologies [1-5]. In particular, organic molecules which contain electron donor (D) and electron acceptor (A) units linked by a π-conjugated bridge (D-π-A molecules as *push-pull* systems) have been the subject of considerable effort for the development of electro-optic switching elements for telecommunications and optical information processing [6-11]. Remarkable characteristics of such *push-pull* systems are their large β hyperpolarizabilites of D-π-A molecules and the possibility of tuning this property by changing the nature of the bridge and strengths of the donor and acceptor units. Regarding the building blocks, tetrathiafulvalene (TTF) derivatives have been widely used as an efficient electron donor unit for synthesizing TTF-π-A structures with NLO properties. Indeed, after the first example reported 1998, [12] many other TTF-based *push-pull* derivatives with closed-shell electronic structures exhibiting large NLO responses have been described. [13-20] NLO materials with open-shell electronic structures have also aroused the interest of many researchers because of their perspectives [21-26]. Thus, a few years ago some of us reported the second-order nonlinear optical (SONLO) response of a family of polycholotriphenylmethyl (PTM) radical derivatives showing large hyperpolarizabilities β values [27-29]. In addition, PTM radical derivatives act as efficient electron acceptors in front of many donor molecules.

In view of the donors and acceptor capabilities and large NLO properties of both TTF and PTM radical molecules, they could be of high interest to combine both units in a D-π-A molecule and evaluate the SONLO response. Recently it has been reported a D-π-A system based on a PTM radical electron-acceptor linked to a TTF electron-donor through a vinylene bridge[30] that exhibit a reversible switching between a neutral and zwitterionic state in solution through the application of external stimuli such as the polarity of the solvent or temperature.[30-32] In order to study the NLO response of this radical dyad and evaluate the influence of the open-shell character and the length of the bridge, we have synthesized and characterized a family of TTF-π-PTM radical derivatives (**1a-1c**) and their non-radical analogues (**2a-2c**). In this article we present a detailed study of the intramolecular charge transfer dependence on the open-shell structure and on the bridge length of this family of compounds. Moreover, SONLO properties of such dyads have been evaluated by means of the Hyper-Rayleigh Scattering (HRS) technique showing larger β values for the radical dyads and when increasing the spacer conjugation length. In order to further understand the electronic, geometrical and NLO properties of these TTF-π-PTM dyads, theoretical calculations have been carried out.

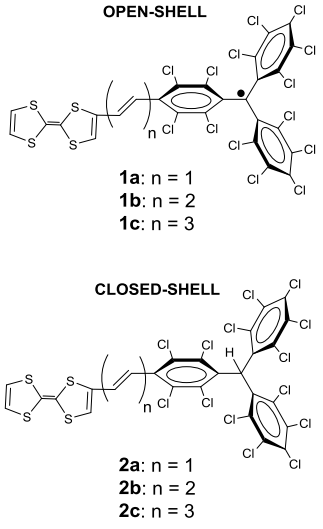

Scheme 1. Molecular structures of D-A radical dyads (**1a**, **1b** and **1c**) and their non-radical derivatives (**2a, 2b and 2c**).

Results and Discussion

1. Synthesis

The synthesis of formyl-TTF precursor **3a** [33,34] was carried out by reaction of monolithio-TTF with dimethylformamide with a yield of 69 %. The improved synthesis of **3b** was reported by González *et al.* [14] and involves the reaction of the monolithio-TTF with N,N-dimethylacrolein to yield the trans-vinylogue amide according to the coupling constants in the ^{1}H-NMR spectra. Finally, the larger formyl-TTF vinylogue **3c** was obtained by a Wittig reaction of **3b** with the phosphorane **4** in a 40 % yield.

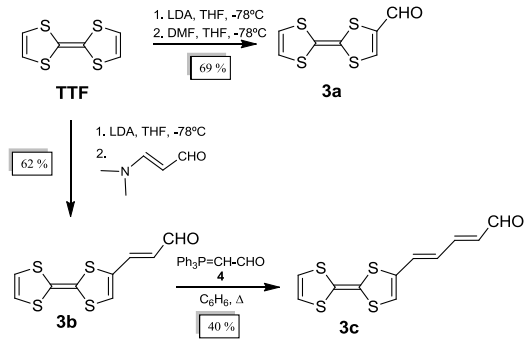

Scheme 2. Synthesis of the formyl-TTF derivatives **3a-3b**.

The synthesis of all non-radical TTF-π-PTM derivatives **2a-2c** was carried out by a Horner-Wadsworth-Emmons reaction of the phosphonated-functionalized non-radical PTM derivative **5** [35] with the formyl-TTF derivatives **3a-3c**. Compounds **2a** and **2b** were obtained in 70 % yield whereas **2c** was obtained in moderate yield (40 %). All-trans vinylogues were obtained according to the coupling constants in the ^{1}H-NMR spectra (see Supporting Information).

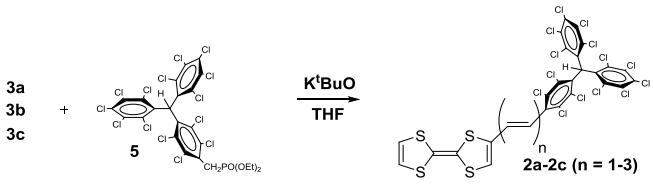

Scheme 3. Synthesis of the compounds **2a-2c**.

Finally, synthesis of radicals **1a-1c** involves the subsequent deprotonation of non-radical TTF-π-PTM derivatives **2a-2c** with tetrabutylammonium hydroxide (TBAOH) followed by oxidation of the formed carbanion with silver nitrate ($AgNO_3$) that afford the final radical dyads **1a-1c** with yields between 73-78% (Scheme 3). The radical compounds were obtained as black solids which are stable under atmospheric conditions.

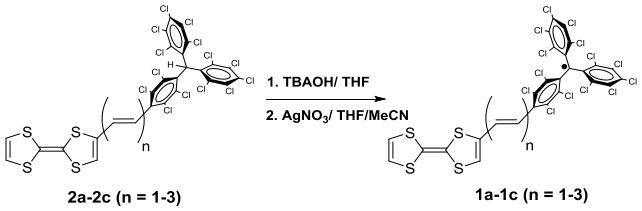

Scheme 3. Synthesis of the radical derivatives **1a-1c**.

2. Electrochemical Properties

Cyclic voltammetry of radicals **1a -1c**, as well as their non-radical precursors **2a -2c**, were performed in CH_2Cl_2 at room temperature (Figures 1 and S4 and Table 1). Spectra of compounds **2a-2c** show two quasi reversible redox waves due to the stepwise oxidation of the TTF moieties to $TTF^{+\cdot}$ and TTF^{2+} with similar redox potentials (vs Ag/AgCl) of around 0.45 and 0.96 V, respectively. As expected the CV of radicals **1a-1c** exhibits three waves, related to the following redox pairs: $PTM^-/PTM\cdot$, $TTF/TTF^{+\cdot}$, and $TTF^{+\cdot}/TTF^{2+}$. It is important to note that the oxidation waves assigned to the TTF moiety are shifted toward more positive values in the case of **1a** than in **2a** suggesting that the radical dyad exhibits a stronger interaction with the donor due to the enhanced electron-acceptor character of the PTM radical moiety. Moreover, this shift gradually increases as the length of the spacer decreases for **1a-1c** indicating a stronger interaction between the donor and acceptor groups when they are closer. On the other hand, the reduction peak assigned to the $PTM^-/PTM^{\cdot}$ process is shifted toward more negative values when the bridge becomes longer.

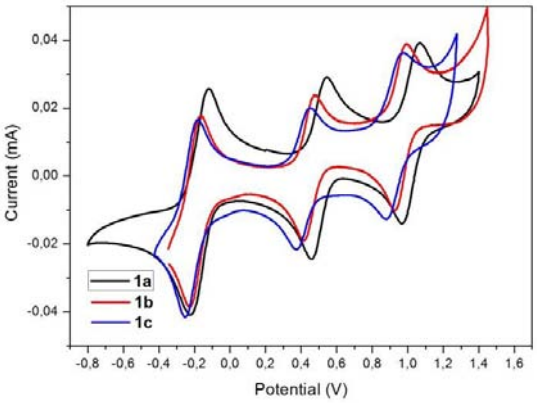

Figure 1. Cyclic voltammetry of solution of radical compounds **1a** (black line), **1b** (red line) and **1c** (blue line) in CH_2Cl_2 vs. Ag/AgCl using *n*-Bu_4PF_6 (0.1 M) as electrolyte at 300 K under argon at a scan rate of 0.1 V/s.

Table 1. CVs data of compounds **1a-1c** and **2a-2c**.

Compound	$E^{red}_{1/2}$	$E^{ox1}_{1/2}$	$E^{ox2}_{1/2}$	ΔE_{red}(V)[b]	ΔE_{ox}(V)[c]
1a	-0.16	0.50	1.01	0.66	0.51
1b	-0.20	0.44	0.96	0.64	0.52
1c	-0.22	0.40	0.92	0.62	0.52
2a	-	0.45	0.95	-	0.50
2b	-	0.45	0.96	-	0.51
2c	-	0.46	0.97	-	0.51

[a] In Volts vs Ag/AgCl; CH_2Cl_2 as solvent, $TBAPF_6$ as electrolyte and scan rate of 0.1 V/s. [b] $\Delta E_{red}(V) = E^{ox1}_{1/2} - E^{red}_{1/2}$. [c] $\Delta E_{ox}(V) = E^{ox2}_{1/2} - E^{ox1}_{1/2}$.

3. Optical Properties

UV-vis spectra of non-radical compounds **2a-2c** in CH_2Cl_2 are showed in the Supporting information (Figure S5). All spectra can be deconvoluted in two principal bands that are shifted towards higher wavelengths as the bridge is increased. We can observe that the calculated HOMO-LUMO gaps from the lowest energy

bands are considerably large (~2 eV) and slightly shifted when increasing the bridge.

More interesting are the UV-Vis-NIR spectra in CH_2Cl_2 of radical compounds **1a-1c** at 300 K (Figure 2) which can be deconvoluted in five principal peaks (See Suporting Information). All spectra show an intense band at 386 nm that is characteristic of PTM radical chromophores. Two unresolved peaks appear at lower energies (426, 456 and 475 nm, and 518, 568 and 607 nm for **1a**, **1b** and **1c** respectively) which are attributed to the electronic conjugation of the unpaired electron into the π-framework. The tendency of these bands is to shift toward lower energies when increasing the bridge length in agreement with the higher electron delocalization over the vinylene units. Finally, we can observe the appearance of broad band between 900-1100 nm that is assigned to an ICT process from the TTF unit to the PTM radical. This band is shifted toward higher energies when increasing the length of oligoenic bridge in agreement with the reduced charge transfer between the donor and the acceptor.

TDDFT calculations have been performed in order to assign each band of dyads **1a-1c** and **2a-2c** to MO transitions (Figures S19 and S20) and to calculate the HOMO-LUMO gaps (Figures S18) observing the same trend as obtained experimentally (Table 2).

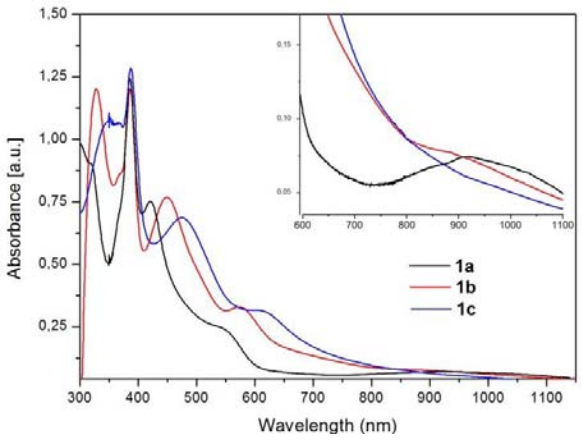

Figure 3. UV-vis-NIR spectra of a solution 0.05 mM of dyads **1a** (black line), **1b** (red line) and **1c** (blue line) in CH_2Cl_2. Inset shows the low-energy range of the absorption spectra of **1a-1c**.

Table 2. UV-vis-NIR data for compounds **1a-1c** and **2a-2c** (lowest energy bands in bold) in CH_2Cl_2. Theoretical and experimental HOMO-LUMO gap calculated from the spectra.

Dyad	λ_{max}/nm ($10^{-3}\varepsilon/M^{-1}\,cm^{-1}$)	exp HOMO-LUMO gap (eV)	theo HOMO-LUMO gap (eV)
1a	295 (20.6); 323 (sh); 385 (26); 426 (15); 518 (4.3); 957 (0.6)	0.96	1.13
1b	273 (sh); 326 (21.8); 385 (29.3); 456 (12.3); 568 (4.5); 942 (0.6)	1.00	1.09
1c	340 (24.9); 385 (30.1); 475 (15.9); 607 (7.4); 918 (0.7)	1.05	1.07
2a	290 (sh); 322 (28.4); 456 (5.4)	2.20	2.65
2b	289 (sh); 332 (26.4); 463 (5.4)	2.15	2.45
2c	278 (sh); 355 (24.8); 471 (6.4)	2.10	2.31

4. Magnetic Properties

ESR spectra of radicals **1a**, **1b** and **1c** in toluene/CH_2Cl_2 (0.05 mM at 220 K show three partially overlapped main lines centered at different *g*-values (Table 3). The shift of such *g*-values indicates a more electron delocalization of the SOMO orbital on the conjugated π-framework. The three overlapped lined observed at 220 K with slightly different hyperfine coupling constants (Table 3) can be ascribed to the coupling of the unpaired electron with two equivalent ^1H atoms of the vinylene bridges (Figure 4). DFT calculations confirmed that the unpaired electron is mainly localized in the PTM unit and that the spin density spreads over the bridge upon increasing the bridge length (Figure S15).

Table 3. ESR parameters used for the simulation of experimental X-band spectra of **1a-1c** radicals.

Compound	*g-value*	a_1(H) (G)
1a	2.0025	1.10
1b	2.0026	1.07
1c	2.0028	1.04

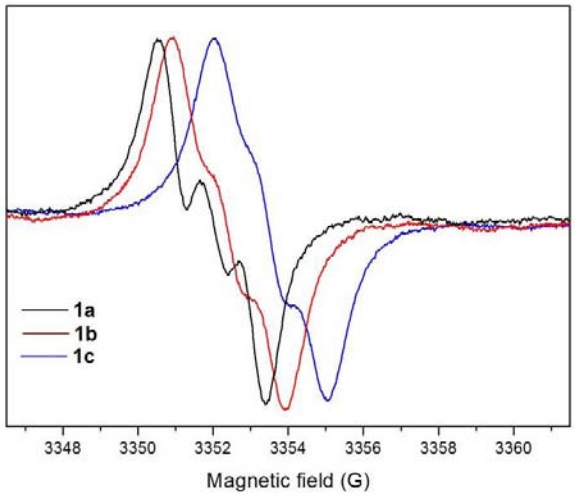

Figure 4. ESR spectra of 0.05 mM solution of dyads **1a** (black line), **1b** (red line) and **1c** (blue line) in toluene/CH_2Cl_2 at 220 K.

5. IR and Raman spectra

In order to gauge the degree of intramolecular charge transfer of **1a-1c** and **2a-2c** systems we have performed an IR and Raman study (See Figures S8 and S9 respectively). The IR bands around 1600 cm^{-1} are assigned to the C=C stretching of the vinylene units and are shifted toward lower frequencies when the bridge length is increased that can be due to the enhanced C=C/C-C conjugation that decreases the multiple bond character of the vinylene units. On the other hand, bands between 900-1000 cm^{-1} are assigned to the C=C-H out of plane bending of the vinylene units in *trans*-position which are shifted towards higher frequencies when the bridge length is increased. Moreover, these shifts are more pronounced in the case of radical dyads **1a-1c** as the electron delocalization in such compounds is enhanced.

Vibrational spectroscopy can also be useful to give us information about the degree of ICT of *push-pull* chromophores. The Raman spectra of dyads **1a-1c** were recorded at 300 K by using an excitation wavelength of λ=514 nm. Raman lines around 1605-1590 cm^{-1} are related to the ν(C=C) stretching mode of the vinyelene unit whereas the bands between 1570-1540 cm^{-1} can be attributed to the ν_4(C=C) stretching mode of the TTF donor unit.[14] The band related to the external spin bearing PTM moiety is reported at 1509 cm^{-1} for the PTM without substituents and shifts towards higher frequencies when PTM radical exerts a more profound electron withdrawal over a richer electron donor unit.[36] In this case, we can observe that this band appears at 1516, 1513 and 1508 cm^{-1} for **1a**, **1b** and **1c**, respectively (Figure 5 and S10), in agreement with the higher degree of charge transfer from the TTF electron donor to the PTM radical acceptor unit as the bridge becomes shorter. Moreover, the band related to the TTF group is upshifted when increasing the length of the π-bridge (from 1552 to 1569 cm^{-1} for **1a** and **1c**, respectively) indicating a higher degree of the charge transfer in the TTF unit for the shortest dyad **1a** as it has been already observed for similar TTF derivatives.[14] This is in agreement with the calculated Mulliken charges showing that the TTF unit donates more electron density as the bridge becomes shorter (Figure S16).

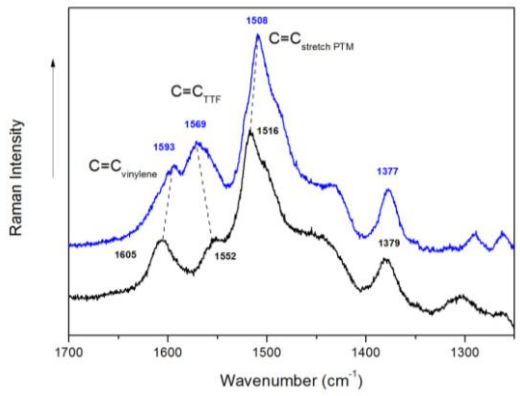

Figure 5. Raman spectra of dyads **1a** (black line) and **1c** (blue line) at λ=514 nm.

Table 4. IR data of selected frequencies

Compound	C=C$_{VIN}$ stretch (ν cm^{-1})	C=C$_{TTF}$ stretch (ν cm^{-1})	C=C$_{VIN}$ bend (ν cm^{-1})
1a	1601	1493	938
1b	1594	1508	971
1c	1571	1508	989
2a	1611	1515	943
2b	1595	1512	978
2c	1575	1509	989

6. Second-Order Non-linear Optical Properties

In order to evaluate the NLO properties of **1a-1c** and **2a-2c** we have performed HRS measurements using a laser system based on Ti:sapphire regenerative amplifier, which is pumping an optical parametric amplifier, allowing the output to be tuned in the wavelength range from 300 nm to 3 μm. A. Molecular nonlinear coefficients of compounds **1a-1c** and **2a-2c** were determined in $CHCl_3$ solution at room temperature using HRS technique with a wavelength of λ = 1550 nm. A worth noticing point of the experimental values is the large increase of β values of radical compounds in comparison with the non-radical ones that ranges from 2.5 to 10 times. Moreover, there is an increase of the hyperpolarizability when the bridge length is enlarged in accordance with the enhancement of the electronic delocalization. The same trend is observed in the calculated hyperpolarizabilitites showing higher relative β values when the bridge becomes larger (Figures S21 and S22).

Table 5. Experimental and calculated NLO properties of compounds **1a-1c** and **2a-2c**.

Compound	exp β (10^{-30}esu)[a]	theo β (10^{-30}esu) (B3LYP/6-31G**)
1a	440	2500
1b	600	3500
1c	880	4500
2a	49	10
2b	90	250
2c	175	510

[a] Measured in $CHCl_3$ at 1550 nm.

Conclusions

In summary, we have reported the synthesis of a new family of TTF-π-PTM dyads that have been fully characterized by multiple spectroscopic techniques in order to analyze the intramolecular charge transfer between the electron-donor TTF and the electron-acceptor PTM radical. In addition, the second-order non-linear optical (NLO) of the radical dyads derivatives have been studied using the HRS technique demonstrating a direct dependence on the bridge length as well on the open-shell structure comparing with their non-radical analogues. Moreover, theoretical calculations have been performed in order to further understand the electronic, geometrical and NLO properties of such TTF-π-PTM dyads.

ASSOCIATED CONTENT

Supporting Information. General methods for synthesis and characterization, synthesis and characterization of **3a-3c**, **2a-2c** and **1a-1c**, UV-vis spectra of **2a-2c**, deconvoluted UV-vis-NIR spectra of **1a-1c**, IR spectra of **2a-2c** and **1a-1c**, Raman spectra of **2a-2c** and **1a-1c**, theoretical calculations.

AUTHOR INFORMATION

Corresponding Author

* E-mail: vecianaj@icmab.es

Notes

The authors declare no competing financial interest.

ACKNOWLEDGMENT

This work was supported by the DGI grant (POMAs (CTQ2010-19501), the Networking Research Center on Bioengineering, Biomaterials, and Nanomedicine (CIBER-BBN), and the Generalitat de Catalunya (grant 2009SGR00516). M.S. is grateful to MEC for a FPU predoctoral grant and he is enrolled in the Material Science Ph.D. program of UAB. We thank Amable

Bernabé for MALDI spectroscopy. We thank Vega Lloveras for ESR spectroscopy.

REFERENCES

(1) Chemla, D. S., Zyss, J., Eds.; *Nonlinear Optical Properties of Organic Molecules and Crystals*; Academic Press: New York, **1987**.

(2) J. Zyss (Ed.), *Molecular Nonlinear Optics*, Academic Press, New York, **1994**.

(3) N.P. Prasad, D.J. Williams, Introduction to Nonlinear Optical Effects in Molecules and Polymers, New York, Wiley, **1991**.

(4) D. M. Burland; Optical Nonlinearities in Chemistry. Chem. Rev. **1994**, 94 (1).

(5) S. R. Marder, B. Kippelen, A. K.-Y. Jen, N. Peyghambarian; Design and synthesis of chromophores and polymers for electro-optic and photorefractive applications; Nature **1997**, 388, 8452851.

(6) Nonlinear Optics of Organics and Semiconductors; Kobayshi, K., Ed.; Springer: Tokyo, **1989**.

(7) Kanis, D. R.; Ratner, M. A.; Marks, T. J. Chem. Rev. **1994**, 94, 195.

(8) Long, N. J. Angew. Chem., Int. Ed. Engl. **1995**, 34, 21.

(9) I. Asselberghs; K. Clays; A. Persoons; M. D. Ward; J. McCleverty. J. Mater.Chem., 2004, 14, 2831-2839.

(10) Stegeman, G. I.; Stegeman, R. A. Nonlinear Optics: Phenomena, Materials and Devices; Wiley: Hoboken, NJ, **2012**.

(11) M. Shimada; Y. Yamanoi; T. Monosori; T. Kondo; E. Nishibori; A. Hatakeyama; K. Sugimoto; H. Nishihara. *J. Am. Chem. Soc.* **2015**, 137, 1024−1027

(12) A. I. de Lucas, N. Martín, L. Sánchez, C. Seoane, R. Andreu, J. Garín, J. Orduna, R. Alcalá, B. Villacampa. *Tetrahedron Lett.,* **1998**, 54, 4655-4662.

(13) Bryce, M. R.; Green, A.; Moore, A. J.; Perepichka, D. F.; Batsanov, A. S.; Howard, J. a K.; Ledoux-rak, I.; Gonza, M.; Segura, L. J.; Garı, J.; Alcala, R. *European J. Org. Chem.* **2001**, 1927–1935.

(14) González, M.; Segura, L.; Seoane, C.; Martín, N.; Garín, J.; Alcala, R.; Lo, J. T. **2001**, 8872–8882.

(15) J. L. Segura; N. Martín. *Angew. Chem. Int. Ed.* **2001**, 40, 1372.

(16) S. Alías, R. Andreu, M. Jesús Blesa, S. Franco, J. Garín, A. Gragera, J. Orduna, P. Romero, B. Villacampa, M. Allain. *J. Org. Chem.* **2007**, 72, 6440-6446.

(17) Alías, S.; Andreu, R.; Blesa, M. J.; Cerdán, M. A.; Franco, S.; Garin, J.; López, C.; Orduna, J.; Sanz, J.; Alicante, R.; Villacampa, B.; Allain, M. *J. Org. Chem.* **2008**, *73* (15), 5890–5898.

(18) Liu, C. G.; Guan, W.; Song, P.; Yan, L. K.; Su, Z. M. *Inorg. Chem.* **2009**, *48* (14), 6548–6554.

(19) Liu, C.-G.; Guan, X.-H. *Phys. Chem. Chem. Phys.* **2012**, *14* (15), 5297.

(20) Si, Y.; Yang, G.; Su, Z. *J. Mater. Chem. C* **2013**, *1* (7), 1399–1406.

(21) Nicoud, J.-F.; Serbutoviez, C.; Puccetti, G.; Ledoux, I.; Zyss, J. *Chem. Phys. Lett.* **1990**, *175* (3), 257–261.

(22) Radicals, M. N.; Angeloni, L.; Caneschi, A.; David, L.; Fabretti, A.; Ferraro, F.; Sessolib, R. **1994**, *4* (1), 1047–1053.

(23) Bella, S. Di; Fragala, I.; Ledoux, I.; Marks, T. J. *J. Am. Chem. Soc.* **1995**, *117* (4), 9481–9485.

(24) Di Bella, S.; Fragalà, I.; Marks, T. J.; Ratner, M. a. *J. Am. Chem. Soc.* **1996**, *118* (50), 12747–12751.

(25) Yoneda, K.; Nakano, M.; Fukuda, K.; Matsui, H.; Takamuku, S.; Hirosaki, Y.; Kubo, T.; Kamada, K.; Champagne, B. *Chem. - A Eur. J.* **2014**, No. Vci, 11129–11136.

(26) M. Nakano; B. Champagne. *J. Phys. Chem. Lett.*, **2015**, *6* (16), 3236–3256.

(27) I. Ratera; S. Marcen; S. Montant; D. Ruiz-Molina; C. Rovira; J. Veciana; J.-F. Létard; E. Freysz. *Chem. Phys. Lett.*, **2002**, 363, 245–251.

(28) I. Ratera, D. Ruiz-Molina, C. Sporer, S. Marcen, S. Montant, J.-F. Létard, E. Freysz, C. Rovira, J. Veciana. *Polyhedron*, **2003**, 22, 1851-1856.

(29) C. Sporer, I. Ratera, D. Ruiz-Molina,Y. Zhao, J.Vidal-Gancedo, K. Wurst, P. Jaitner, K. Clays, A. Persoons, C.Rovira, J. Veciana. *Angew. Chem. Int. Ed.* **2004**, 43, 5266 –5268

(30) Guasch, J.; Grisanti, L.; Lloveras, V.; Vidal-Gancedo, J.; Souto, M.; Morales, D. C.; Vilaseca, M.; Sissa, C.; Painelli, A.; Ratera, I.; Rovira, C.; Veciana, J. *Angew. Chemie - Int. Ed.* **2012**

(31) Guasch, J.; Grisanti, L.; Souto, M.; Lloveras, V.; Vidal-Gancedo, J.; Ratera, I.; Painelli, A.; Rovira, C.; Veciana, J. *J Am Chem Soc* **2013**.

(32) Souto, M.; Guasch, J.; Lloveras, V.; Mayorga, P.; López Navarrete, J. T.; Casado, J.; Ratera, I.; Rovira, C.; Painelli, A.; Veciana, J. *J. Phys. Chem. Lett.* **2013**.

(33) D. C. Green, *J. Org. Chem.* **1979**, 44, 1476 – 1479.

(34) J. Garín, J. Orduna, S. Uriel, A. J. Moore, M. R. Bryce, S. Wegener, D. S. Yufit, J. A. K. Howard, *Synthesis* **1994**, 489 – 493.

(35) C. Rovira, D. Ruiz-Molina, O. Elsner,J.Vidal-Gancedo, J. Bonvoisin, J.-P. Launay, J.Veciana, *Chem. Eur. J.*, **2001**, 7, 240–250.

(36) S. R. González, B. Nieto-Ortega, R. C. González Cano, V. Lloveras, J. J. Novoa,F.Mota, J. Vidal-Gancedo, C. Rovira, J. Veciana, E. Del Corro, M. Taravillo, V. G. Baonza, J. T. López Navarrete, J. Casado, J. Chem. Phys. 2014, 140,164903/1-164903/9.

Nonlinear Optical Properties of Push-Pull TTF-p-PTM Radicals: the Role of the Open-Shell Structure and Bridge Length

Manuel Souto,[†] Valentina Pia,[‡] Imma Ratera,[†] Enrique Ortí,[⊥] Wim Wenseelers,[‡] and Jaume Veciana[†,*]

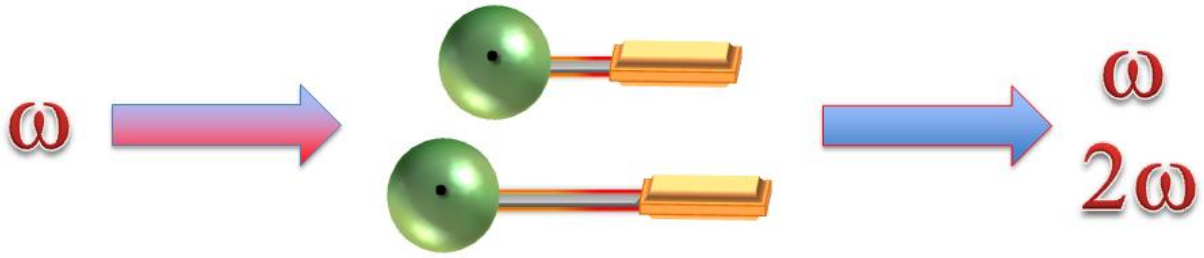

Supporting Information

Non-Linear Optical Properties of push-pull TTF-π-PTM Radicals: the role of the bridge length and the open-shell structure

Manuel Souto,[†] Valentina Pia,[‡] Imma Ratera,[†] Enrique Ortí,[⊥] Wim Wenseelers,[‡] and Jaume Veciana[†,*]

[†] Institut de Ciència de Materials de Barcelona (ICMAB-CSIC)/CIBER-BBN, Campus Universitari de Bellaterra, 08193 Cerdanyola del Vallès (Barcelona), Spain
[‡] Department of Physics, University of Antwerp (campus Drie Eiken), Universiteitsplein 1, B-2610 Wilrijk-Antwerpen, Belgium
[⊥] Instituto de Ciencia Molecular, Universidad de Valencia, 46980 Paterna, Spain

Contents

General methods for synthesis and characterization

^{1}H NMR spectra were recorded using a Bruker Avance 250, 400, 500 instruments and Me4Si as an internal standard. Infrared spectra were recorded with Spectrum One FT-IR Spectroscopy instrument and UV/Vis/NIR spectra were measured using Cary 5000E Varian. ESR spectra were performed with a Bruker ESP 300 E equipped with a rectangular cavity T102 that works with an X-band (9.5 GHz). The solutions were degassed by argon bubbling before the measurements. LDI/TOF MS were recorded in a Bruker Ultraflex LDI-TOF spectrometer. Cyclic voltammetry measurements were obtained with a potentiostat 263a from EG&G Princeton Applied Research in a standard 3 electrodes cell. The HRS measurements were pertformed using a laser system based on Ti:sapphire regenerative amplifier, which is pumping an optical parametric amplifier, allowing the output to be tuned in the wavelength range from 300 nm to 3 μm. All reagents and solvents employed for the syntheses were of high purity grade and were purchased from Sigma-Aldrich Co., Merck, and SDS. Dry solvents were used in the chemical reactions and in the cyclic voltammetries. The solvents used for optical spectroscopy and ESR measurements were of HPLC grade (ROMIL-SpS). In addition, for cyclic voltammetry experiments, CH_2Cl_2 was filtered over basic alumina to eliminate the acidic residues.

Synthesis of 3a: 1.00 g (4.9 mmols) of tetrathiafulvalene, previously recrystallized from heptane, was dissolved in 60 ml of anhydrous THF under an inert atmosphere. Then, it was cooled down to -78 ºC with an acetone/N_2 bath and 3.13 ml of LDA (1.8 M) were added and stirred for 90 minutes to obtain the lithiated TTF-derivative. After that, 1.20 ml (15.5 mmols) of anhydrous *N*,*N*-dimethylformamide (DMF) were added in the solution which was stirred for 2 extra hours. Then, the mixture was acidified with hydrochloridric acid (2 M), extracted with CH_2Cl_2, and washed with water. The organic phase was dried with anhydrous magnesium sulfate, filtrated, and the solvent was evaporated under reduced pressure. The product was purified by column chromatography of silica gel using a mixture of hexane and CH_2Cl_2 as eluent (1:1). 0.79 g (69%) of the final product was obtained. **Characterization: LDI-TOF** (positive mode): *m/z* (amu/e$^-$): 233.37 ($M^{+\cdot}$) **^{1}H-RMN** (250MHz, CDCl3, δ (ppm)): 9.48 (s, 1H, CHO); 7.43 (s, 1H, CH); 6.33 (s, 2H, CH). **FT-IR** (ν cm^{-1}): 3267 (w); 3063 (w); 3038 (w); 2920 (w); 2281 (w); 2114 (w); 1786 (w); 1713 (w); 1662 (s); 1645 (s); 1561 (m); 1550 (m); 1532 (s); 1515 (s); 1472 (m); 1368 (m); 1287 (m); 1252 (m); 1228 (m); 1143 (s); 1075 (m); 1000 (m); 983 (m); 866 (w); 829 (m); 788 (s); 775 (s); 737 (m); 697 (m).

Synthesis of 3b: 550 mg (2.70 mmol) of tetrathiafulvalene were dissolved in 40 ml of anhydrous THF under Ar atmosphere. Then it was cooled to -78 °C and 1.70 ml of a 2 M solution of lithium diisopropylamide (LDA) in tetrahydrofuran were added to the solution and stirred for 60 minutes. Then, 0.5 ml (5.2 mmol) of 3-(dimethylamino)-acrolein was added and the solution was stirred for two hours. Afterward, the mixture was acidified with hydrochloric acid (2 M), extracted with CH_2Cl_2 and washed with water. The organic phase was dried with anhydrous magnesium sulfate, filtrated and the solvent was evaporated under reduced pressure. The product was purified by column chromatography of silica gel using a mixture of hexane and ether to yield 430 mg (62%) of TTF-CH=CH-CHO (**3b**) as a dark red-brownish solid. **Characterization**: **^{1}H-NMR** (250 MHz, $CDCl_3$, δ(ppm)): 9.58 (d, 1H, J = 7.4 Hz, C**H**O); 7,17 (d, 1H, J = 15.4 Hz, C**H**-CHO); 6.87 (s, 1H); 6.35 (s, 2H); 5.96 (dd, 1H, J = 15.4, 7.4 Hz, CH=C**H**-CHO). **FT-IR** (ν cm^{-1}): 3063 (w); 2955 (w); 2921 (m); 2851 (m); 1738 (w); 1660 (s, **C=O**); 1600 (s, CH=CH); 1522 (m); 1511 (m); 1458 (w); 1382 (w); 1252 (w); 1216 (w); 1157 (w); 1112 (s); 1001 (w); 953 (s); 830 (m); 795 (m) 754 (s); 728 (m); 669 (m). **LDI-TOF** (positive mode): *m/z* (amu/e$^-$): 257.722 ($M^{+\cdot}$).

Synthesis of 3c: A solution of triphenylphosphoranylidene-acetaldehyde (212 mg, 0.7 mmol) and **3b** (90 mg, 0.35 mmol) in benzene (20 ml) was refluxed under Ar for 3 hours. After cooling, hexane (30 ml) was added and the precipitated Ph_3PO was filtered. The solvent was evaporated and the product was purified by column chromatography using hexane/Et_2O (90:10) to obtain 40 mg (40 %) of TTF-CH=CH-CH=CH-CHO (**3c**) as a red solid. **Characterization**: **^{1}H-NMR** (250 MHz, $CDCl_3$, δ(ppm)): 9.57 (d, 1H, J = 7.9 Hz, C**H**O); 7,10 (dd, 1H, J = 15.2, 11.0 Hz); 6.73 (d, 1H, J = 15.1 Hz); 6.59 (s, 1H); 6.33 (s, 2H); 6,26

(dd, 1H, J = 14.5, 11.2 Hz); 6,20 (dd, 1H, J = 14.5, 7.6 Hz). **FT-IR** (ν cm^{-1}): 3063 (w); 2981 (w); 2848 (w); 1660 (s, **C=O**); 1602 (s, CH=CH); 1582 (s, CH=CH); 1504 (s); 1392 (w); 1289 (w); 1246 (w); 1140 (s); 1108 (s); 1006 (m); 975 (s); 830 (w); 795 (m); 776 (m); 750 (m). **LDI-TOF** (positive mode): *m/z* (amu/e^-): 283.352 ($M^{+\cdot}$).

Synthesis of 2a: 1000 mg (1.14 mmols) of the phosphonate PTM derivative (4-[bis(2,3,4,5,6-pentachlorophenylmethyl)methyl]-2,3,4,6-tetrachlorobenzyl phosphonate) were dissolved in 40 ml of anhydrous THF under strict inert conditions. The solution was cooled down to -78 ºC by means of an acetone/CO_2(s) bath. Next, 384 mg (3.42 mmols) of potassium *tert*-butoxide were added and stirred for 20 minutes to form the yellow ylide under an inert argon atmosphere. After that, 141 mg (1.25 mmols) of formyl-TTF were added and the reaction was kept at a low temperature under argon for 3 days. Then, the solution was slowly warmed up to RT and acidified with 1.7 ml of a 2 M solution of HCl and the product was extracted with 3 portions of 40 ml of CH_2Cl_2. The organic phase was washed with water, dried with anhydrous magnesium sulfate and the solvent was evaporated under reduced pressure. Finally, the product was purified by flash column chromatography of silica gel using a mixture of hexane/diethyl ether (50:50) as eluent. 778 mg (80%) of product 1-H were obtained. **Characterization**: **^{1}H-NMR** (250 MHz, C_6D_6, δ(ppm)): δ=7.21 (s, 1H; PTM-H), 6.29 (d, 1H, J = 16.0 Hz); 6.13 (d, 1H, J = 16.2 Hz); 5.52 (s, 1H); 5.39 (s, 2H). **FT-IR** (KBr, ν (cm^{-1})): 2925 (s), 2850 (s), (C-H TTF); 1610 (s) (vinylene bridge); 1530 (m), 1513 (m) (C=C TTF); 1463 (m); 1356 (s); 1336 (s); 1296 (s); 1134 (m); 1120 (m); 943 (m); 794(s), 779 (s) (C-Cl); 752 (m). **UV-VIS-NIR** (CH_2Cl_2, λ_{max} in nm, $10^{-3}\varepsilon$ in $M^{-1}\cdot cm^{-1}$): 290 (sh); 322 (28.4); 456 (5.4). **LDI-TOF** (negative mode): *m/z* (amu/e^-): 953.705 ($M^{-\cdot}$). **Cyclic voltammetry** (Bu_4NPF_6 0.15 M in CH_2Cl_2 as electrolyte): E½=0,448 V and E½=0,965 V vs. Ag/AgCl.

Synthesis of 2b: 454 mg (0.52 mmol) of the phosphonated PTM derivative were dissolved in 40 ml of anhydrous THF under inert conditions. The solution was cooled down to -78 ºC and 116 mg (1.03 mmol) of potassium *tert*-butoxide were added and stirred for 20 minutes to form the yellow-orange ylide. After 20 minutes, 147 mg (0.57 mmol) of the aldehyde **3b** were added and the reaction was warmed up to room temperature and stirred for 2 days. Then the mixture was extracted with CH_2Cl_2, washed with water, dried with anhydrous $MgSO_4$ and solvents were evaporated under reduced pressure. Finally the product was purified by column chromatography of silica gel using a mixture of ether and hexane (1:1) to obtain to obtain 362 mg (71 %) of **2b** as a dark reddish powder. **Characterization**: **^{1}H-NMR** (250 MHz, C_6D_6, δ(ppm)): 7.23 (s, 1H); 6.49 (dd, 1H, J = 15.7, 10.5 Hz); 6,30 (d, 1H, J = 15.7 Hz); 6.09 (dd, 1H, J=15.2, 10.0 Hz); 5.87 (d, 1H, J=15.1 Hz); 5.50 (s, 1H); 5.41 (s, 2H). **FT-IR** (ν cm^{-1}): 2951 (w); 2922 (m); 2851 (m); 1727 (w); 1597 (m, CH=CH); 1526 (m); 1513 (m); 1458 (w); 1369 (w); 1337 (m); 1294 (s); 1239 (w); 1190 (w); 1136 (m); 979 (s); 922 (w); 859 (w); 828 (w); 806 (s); 793 (s); 778 (m); 746 (w); 734 (w); 685 (m). **UV-VIS-NIR** (CH_2Cl_2, λ_{max} in nm, $10^{-3}\varepsilon$ in $M^{-1}\cdot cm^{-1}$): 289 (sh); 332 (26.4); 463 (5.4). **LDI-TOF** (positive mode): *m/z* (amu/e^-): 981.705 ($M^{+\cdot}$). **Cyclic voltammetry** (Bu_4NPF_6 0.15 M in CH_2Cl_2 as electrolyte): $E_{½}^1$= 0.447 V; $E_{½}^2$=0.958 V.

Synthesis of 2c: 230 mg (0.26 mmol) of the phosphonated PTM derivative were dissolved in 30 ml of anhydrous THF under inert conditions. The solution was cooled down to -78 ºC and 60 mg (0.52 mmol) of potassium *tert*-butoxide were added and stirred for 20 minutes to form the yellow-orange ylide. After 20 minutes, 85 mg (0.30 mmol) of the aldehyde **3c** were added and the reaction was warmed up to room temperature and stirred for 2 days. Then the mixture was extracted with CH_2Cl_2, washed with water, dried with anhydrous $MgSO_4$ and solvents were evaporated under reduced pressure. Finally the product was purified by column chromatography of silica gel using a mixture of ether and hexane (1:1) to obtain to obtain 105 mg (40 %) of **2c** as a dark reddish powder. **Characterization**: **^{1}H-NMR** (250 MHz, C_6D_6, δ(ppm)): 7.23 (s 1H); 6.64 (dd, 1H, J = 15.6, 9.6 Hz,); 6.36 (d, 1H, J = 15.5 Hz); 6.1-5.8 (m, 4H); 5.51 (s, 1H); 5.42 (SM 2H). **FT-IR** (ν cm^{-1}): 2955 (w); 2922 (w); 2855 (w); 1575 (m, CH=CH); 1525 (m); 1510 (m); 1459 (m); 1370 (w); 1337 (m); 1294 (s); 1237 (w); 1138 (m); 992 (s); 951 (w); 859 (w); 808 (s); 778 (m); 735 (w); 716 (w); 682 (m). **LDI-TOF** (negative mode): *m/z* (amu/e^-): 1004.488 ($M^{-\cdot}$); (positive

mode): *m/z* (amu/e$^-$): 1003.931 ($M^{\cdot-}$). **UV-VIS-NIR** (CH_2Cl_2, λ_{max} in nm, $10^{-3}\varepsilon$ in $M^{-1}\cdot cm^{-1}$): 278 (sh); 355 (24.8); 471 (6.4). **Cyclic voltammetry** (Bu_4NPF_6 0.15 M in CH_2Cl_2 as electrolyte): $E_{½}^1$=0.462 V; $E_{½}^2$=0.970 V.

Synthesis of 1a: 100 mg (0.1 mmol) of **2a** were dissolved in 30 ml of anhydrous THF. 150 µl (0.15 mmol) of tetrabutylammonium hydroxide 1.0 M in methanol were added and the purple solution was stirred for 1 hour. Then, 32 mg (0.18 mmol) of silver nitrate dissolved in 5 ml of acetonitrile were added to the solution and stirred for 5 minutes. The solution changes from purple to dark brown with silver (Ag^0) precipitated. Then, the solution was filtered through silica and the solvent was evaporated under reduced pressure. Finally, the product was precipitated with MeOH to produce 73 mg of dyad **1a** (73 %) as brownish powder. **Characterization: FT-IR** (KBr, ν(cm^{-1})): 2915 (w), 2889 (w), 1603 (w) (vinylene bridge); 1502 (w), 1474 (w) (C=C TTF); 1375 (m); 1351 (m); 1334 (s); 1284 (m); 1260 (m); 1250 (m); 1163 (m); 1134 (m); 1102 (s); 940 (s); 798(w), 780 (w) (C-Cl). **UV-VIS-NIR** (CH_2Cl_2, λ_{max} in nm, $10^{-3}\varepsilon$ in $M^{-1}\cdot cm^{-1}$): 295 (20.6); 323 (sh); 385 (26); 426 (15); 518 (4.3); 957 (0.6). **LDI/TOF** (positive mode): *m/z* (amu/e$^-$): 952 [$M^{+\bullet}$], 882 [M-2Cl]$^+$. **Elemental Analysis**: Anal. Calcd. for $C_{27}H_5Cl_{14}S_4$ (C_6H_{14}): C, 38.11; H, 1.84; S, 12.33. Found: C, 38.88; H, 1,7; S, 12.20. **CV** (Bu_4NPF_6 0.15 M in CH_2Cl_2 as electrolyte): $E_{½}^1$=-0.16 V; $E_{½}^2$=0.50; $E_{½}^3$=1.01 V vs. Ag/AgCl. **ESR** (CH_2Cl_2/toluene, 220 K): g=2.0025, a_1(H)=1.10 G.

Synthesis of 1b: 80 mg (0.08 mmol) of **2b** were dissolved in 20 ml of anhydrous THF. 120 µl (0.12 mmol) of tetrabutylammonium hydroxide 1.0 M in methanol were added and the purple solution was stirred for 1 hour. Then, 25 mg (0.14 mmol) of silver nitrate dissolved in 5 ml of acetonitrile were added to the solution and stirred for 5 minutes. The solution changes from purple to dark brown with silver (Ag^0) precipitated. Then, the solution was filtered through silica and the solvent was evaporated under reduced pressure. Finally, the product was precipitated with MeOH to produce 60 mg of dyad **1b** (73 %) as brownish powder. **Characterization: FT-IR** (KBr, ν(cm^{-1})): 2955 (m); 2922 (m); 2851 (m); 1594 (w, CH=CH); 1525 (w); 1508 (m); 1458 (w); 1376 (w); 1333 (s); 1259 (m); 1163 (w); 1136 (m); 1117 (m); 1066 (m); 971 (s); 923 (w); 865 (w); 815 (s); 795 (s); 778 (s); 735 (s); 708 (m). **UV-VIS-NIR** (CH_2Cl_2, λ_{max} in nm, $10^{-3}\varepsilon$ in $M^{-1}\cdot cm^{-1}$): 273 (sh); 326 (21.8); 385 (29.3); 456 (12.3); 568 (4.5); 942 (0.6). **LDI/TOF** (positive mode): *m/z* (amu/e$^-$): 979.711 ($M^{+\cdot}$). **Elemental Analysis**: Anal. Calcd. for $C_{29}H_7Cl_{14}S_4$ (C_6H_{14}): C, 39.43; H, 2.06; S, 12.03. Found: C, 38.8; H, 2.00; S, 11.67. **CV** (Bu_4NPF_6 0.15 M in CH_2Cl_2 as electrolyte): $E_{½}^1$=-0.20 V; $E_{½}^2$=0.44; $E_{½}^3$=0.96 V vs. Ag/AgCl. **ESR** (CH_2Cl_2/toluene, 220 K): g=2.0026, a_1(H)=1.07 G.

Synthesis of 1c: 70 mg (0.07 mmol) of **2b** were dissolved in 20 ml of anhydrous THF. 100 µl (0.10 mmol) of tetrabutylammonium hydroxide 1.0 M in methanol were added and the purple solution was stirred for 1 hour. Then, 21 mg (0.12 mmol) of silver nitrate dissolved in 5 ml of acetonitrile were added to the solution and stirred for 5 minutes. The solution changes from purple to dark brown with silver (Ag^0) precipitated. Then, the solution was filtered through silica and the solvent was evaporated under reduced pressure. Finally, the product was precipitated with MeOH to produce 55 mg of dyad **1c** (78 %) as brownish powder. **Characterization: FT-IR** (KBr, ν(cm^{-1})): 2953 (w); 2922 (w); 2850 (w); 1571 (m, CH=CH); 1508 (m); 1459 (m); 1377 (w); 1333 (s); 1318 (s); 1257 (s); 1157 (w); 1137 (m); 116 (w); 989 (s); 941 (m); 913 (w); 816 (s); 808 (s); 795 (m); 779 (w); 735 (m); 708 (m). **UV-VIS-NIR** (CH_2Cl_2, λ_{max} in nm, $10^{-3}\varepsilon$ in $M^{-1}\cdot cm^{-1}$): 340 (24.9); 385 (30.1); 475 (15.9); 607 (7.4); 918 (0.7). **LDI/TOF** (positive mode): (negative mode): *m/z* (amu/e$^-$): 1004.734 ($M^{\cdot-}$); (positive mode): *m/z* (amu/e$^-$): 1003.203 ($M^{\cdot-}$). **Elemental Analysis**: Anal. Calcd. for $C_{31}H_9Cl_{14}S_4$ (C_6H_{14}): C, 40.69; H, 2.12; S, 11.74. Found: C, 40.9; H, 2.5; S, 11.83. **CV** (Bu_4NPF_6 0.15 M in CH_2Cl_2 as electrolyte): $E_{½}^1$=-0.22 V; $E_{½}^2$=0.40; $E_{½}^3$=0.92 V vs. Ag/AgCl. **ESR** (CH_2Cl_2/toluene, 220 K): g=2.0028, a_1(H)=1.04 G.

^{1}H-NMR of 2a:

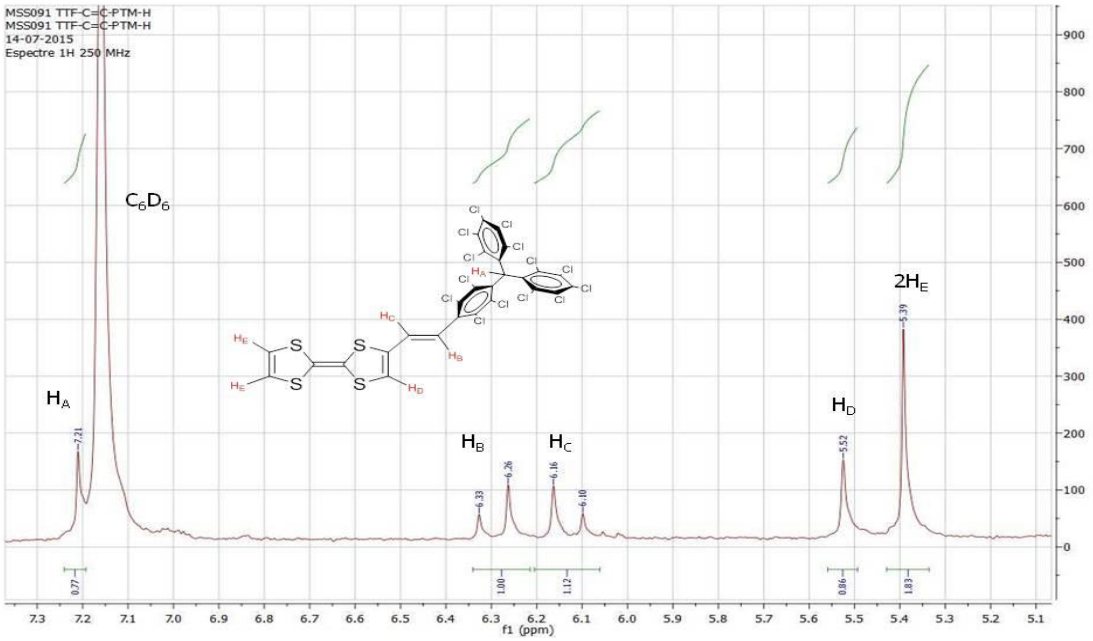

Figure S1. ^{1}H-NMR spectrum of dyad **2a** in C_6D_6 and protons observed in the ^{1}H-NMR spectrum.

^{1}H-NMR of 2b:

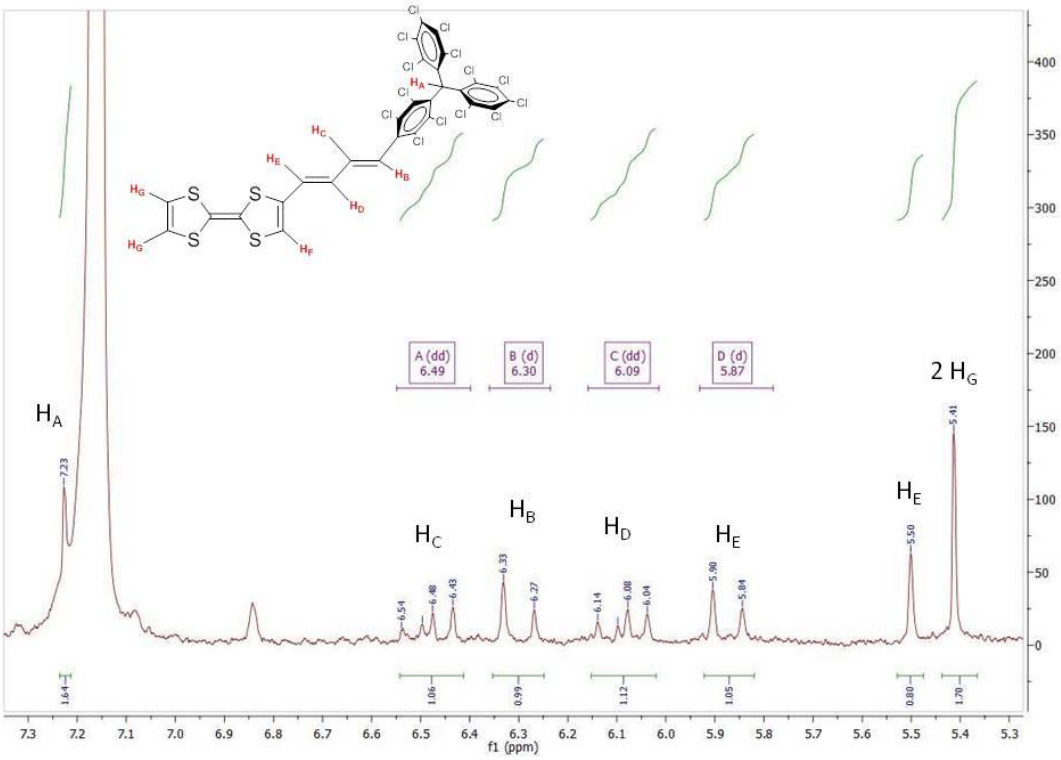

Figure S2. ^{1}H-NMR spectrum of dyad **2b** in C_6D_6 and protons observed in the ^{1}H-NMR spectrum.

[1]H-NMR of 2c:

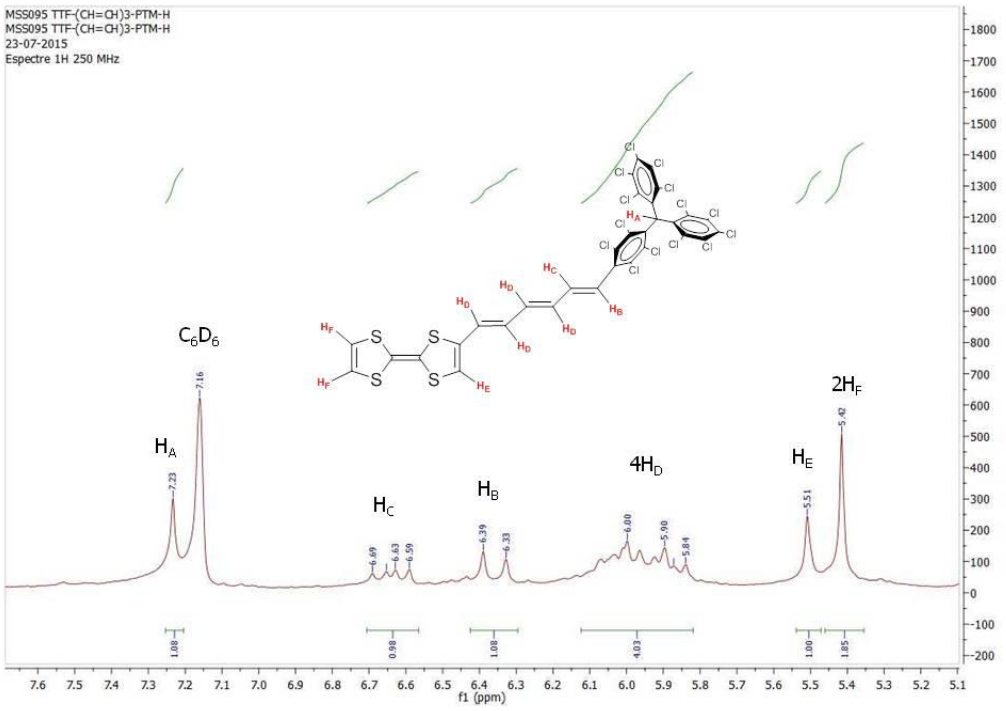

Figure S3. [1]H-NMR spectrum of dyad **2c** in C_6D_6 and protons observed in the [1]H-NMR spectrum.

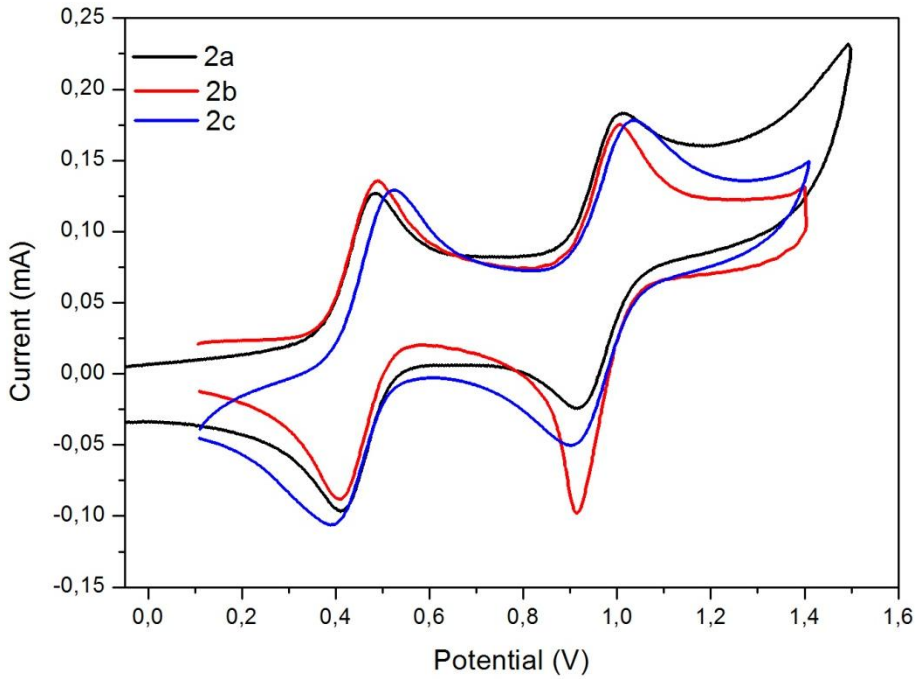

Figure S4. Cyclic voltammetry of solution of compounds **2a** (black line), **2b** (red line) and **2c** (blue line) in CH_2Cl_2 vs. Ag/AgCl using *n*-Bu_4PF_6 (0.1 M) as electrolyte at 300 K under argon at a scan rate of 0.1 V/s.

UV-vis of 2a-2c:

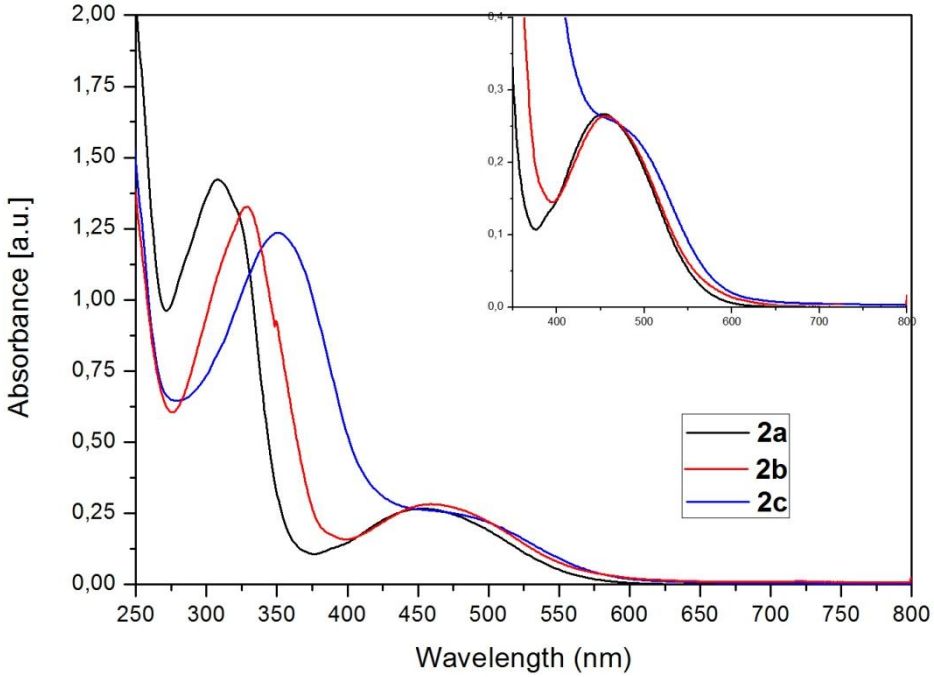

Figure S5. UV-Vis of a solution 0.05 mM of dyads **2a** (black line), **2b** (red line) and **2c** (blue line) in CH_2Cl_2. Inset shows the low-energy range of the absorption spectra of **2a-2c**.

Deconvoluted UV-vis-NIR of 1a-1c:

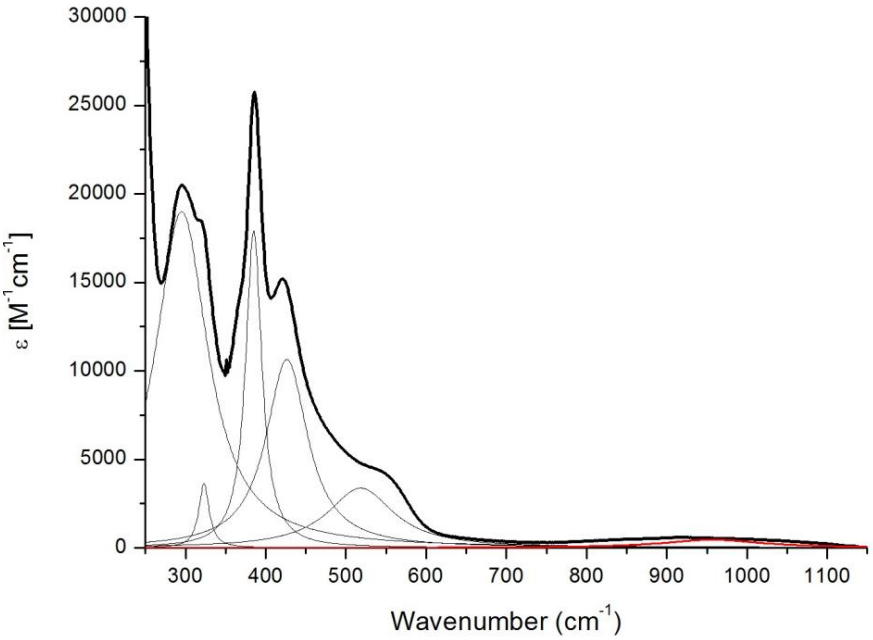

Figure S6. UV-Vis-NIR deconvoluted spectrum of dyad **1a** in CH_2Cl_2.

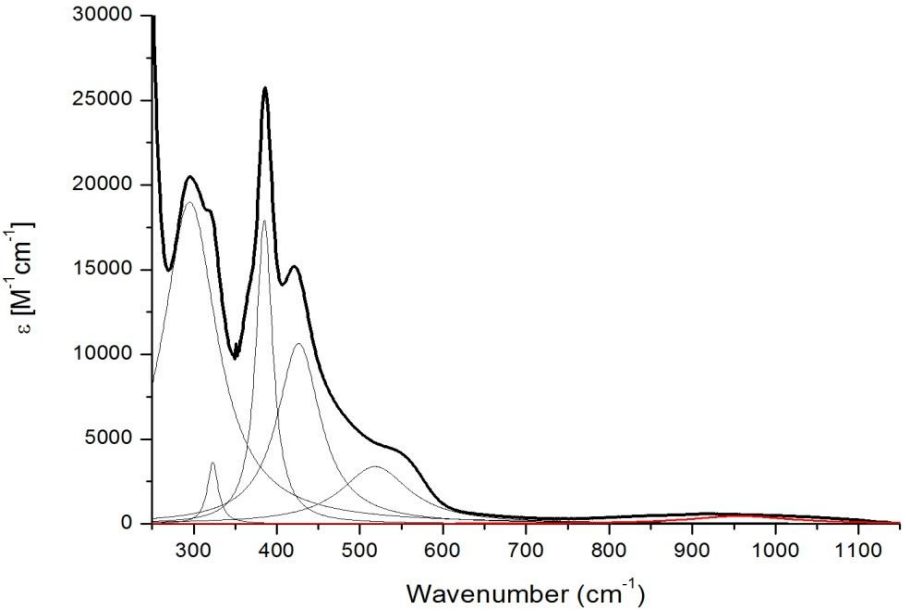

Figure S7. UV-Vis-NIR deconvoluted spectrum of dyad **1b** in CH_2Cl_2.

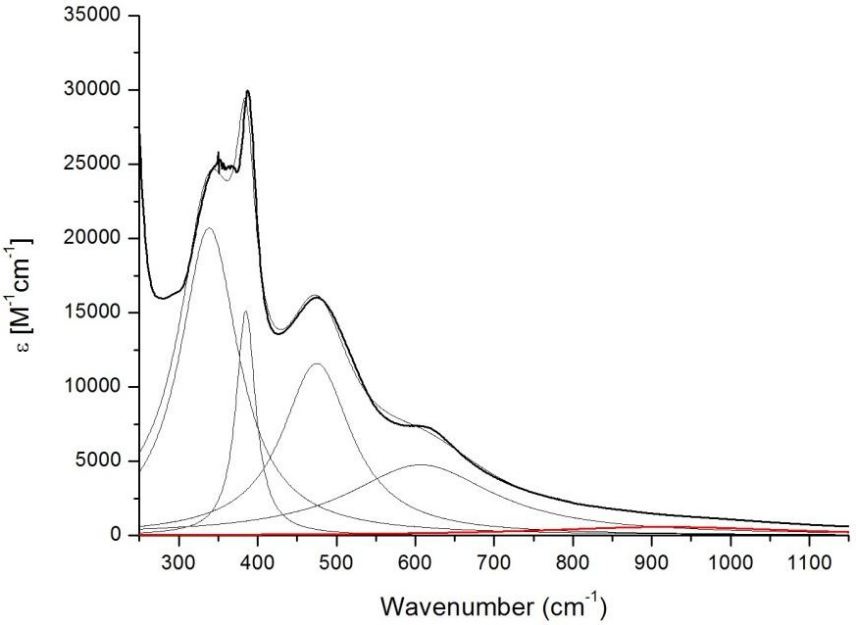

Figure S8. UV-Vis-NIR deconvoluted spectrum of dyad **1c** in CH_2Cl_2.

IR spectra of 2a-2c:

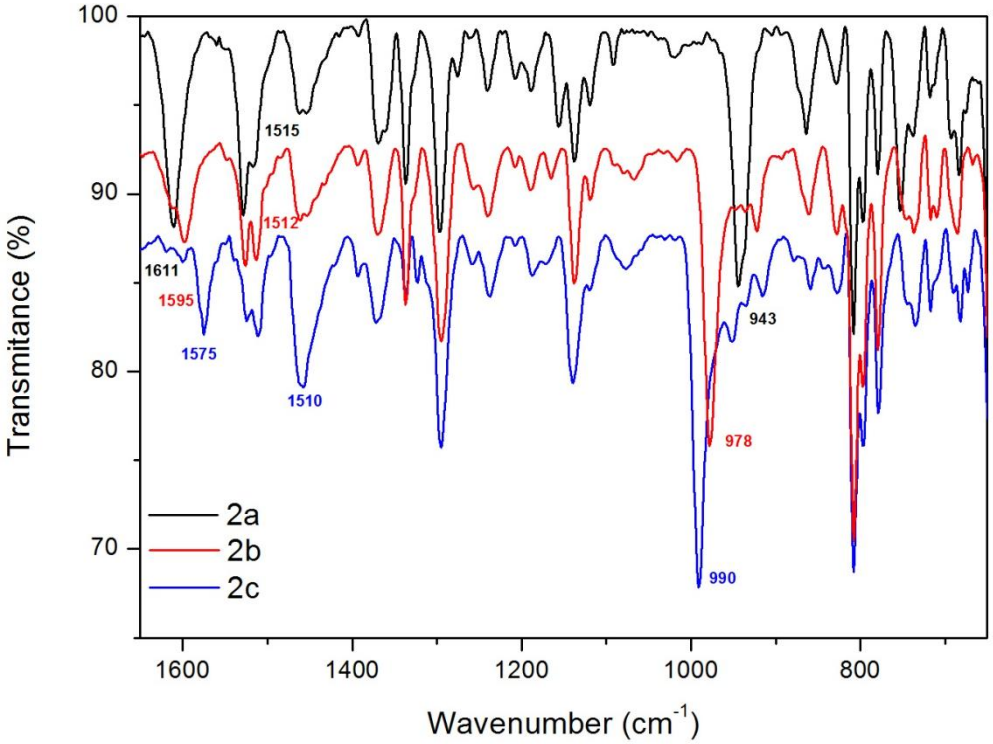

Figure S8. Infrared spectra of compounds **2a-2c**.

IR spectra of 1a-1c:

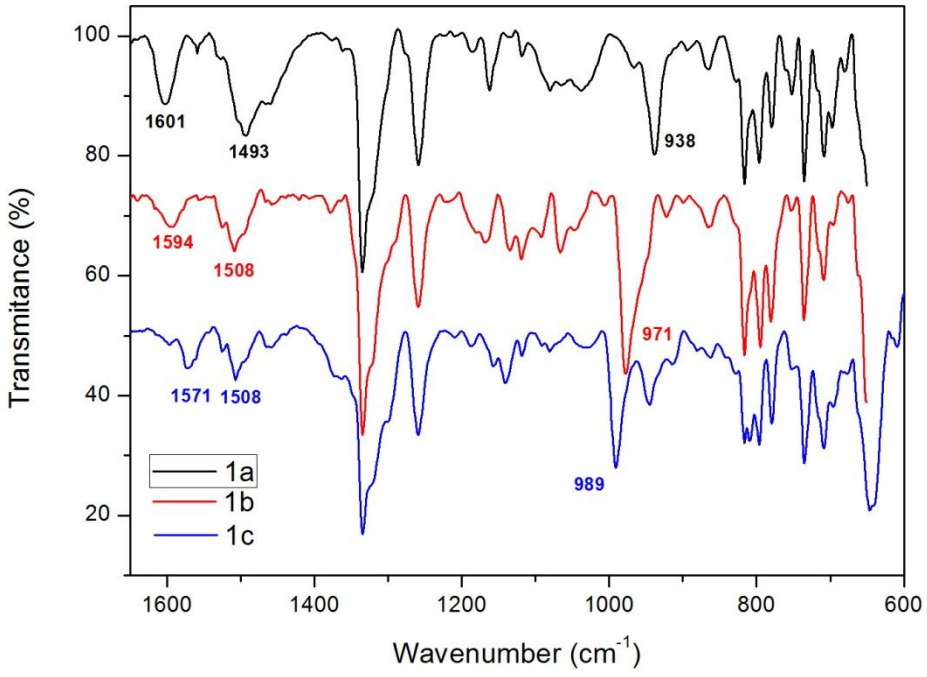

Figure S9. Infrared spectra of compounds **1a-1c**.

Raman spectra of 1a-1c:

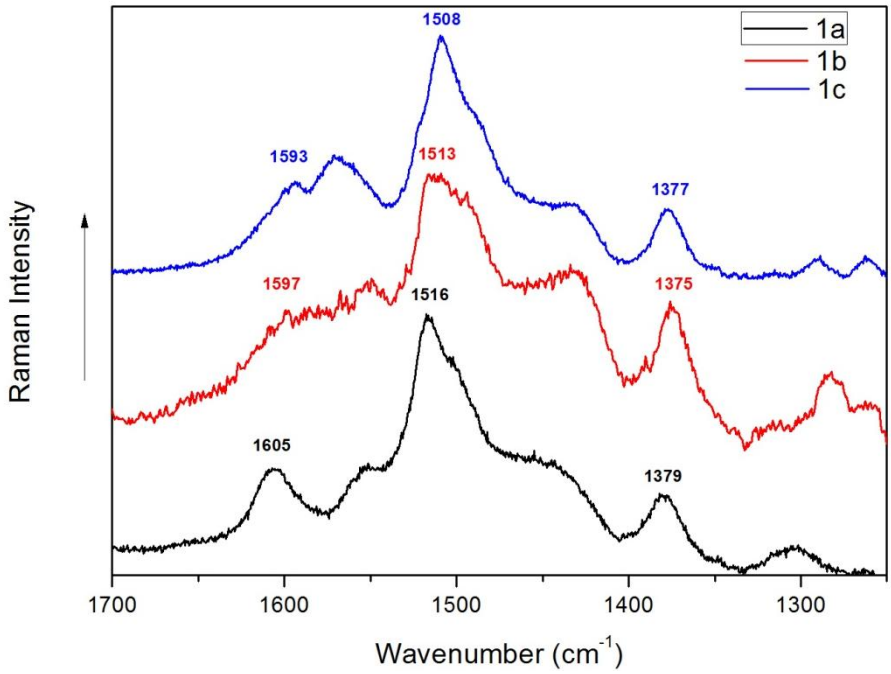

Figure S10. Raman spectra of compounds **1a-1c**.

Computational study of cis/trans conformation of 1a-1c and 2a-2c:

Two main conformers arise from the relative orientation of the TTF unit with respect to the π-conjugated bridge: s-cis isomers (e.g., **2c**) and s-trans isomers (e.g., **2c-t**). The s-trans isomer is calculated ≈3 kcal/mol more stable than the s-cis isomer for all compounds.

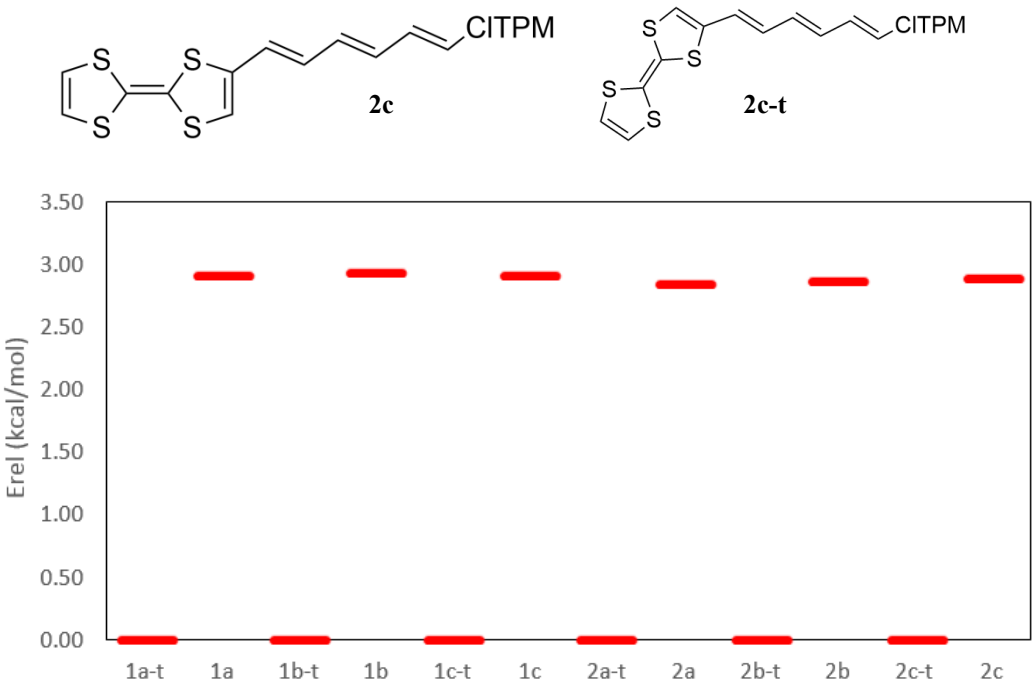

Figure S11. Relative energies for the *cis*- and *trans*- conformers of dyads **1a-1c** and **2a-2c**.

Frontier Molecular Orbitals of Closed-Shell dyads 2a-2c (B3LYP/6-31G) (isovalue = 0.03)**

There are no differences in the frontier MOs between the s-cis and the s-trans isomers. We find an identical MOs picture when using the CAM-B3LYP functional.

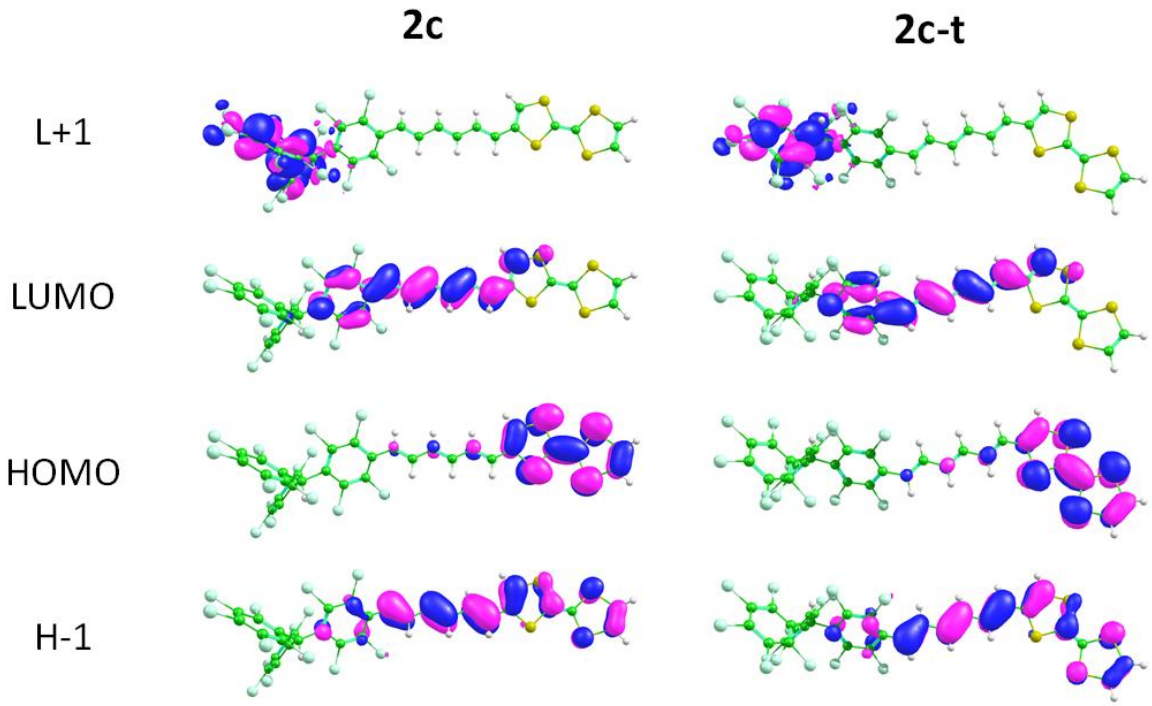

Figure S12. Frontier Molecular Orbitals for the *trans*- and *cis*- conformations of dyad **2c**.

The HOMO is centered on the TTF, and the LUMO+1 is located on the PTM unit. Both orbitals suffer no change upon increasing the length of the bridge. The LUMO and the HOMO-1 spread along the bridge upon increasing its length.

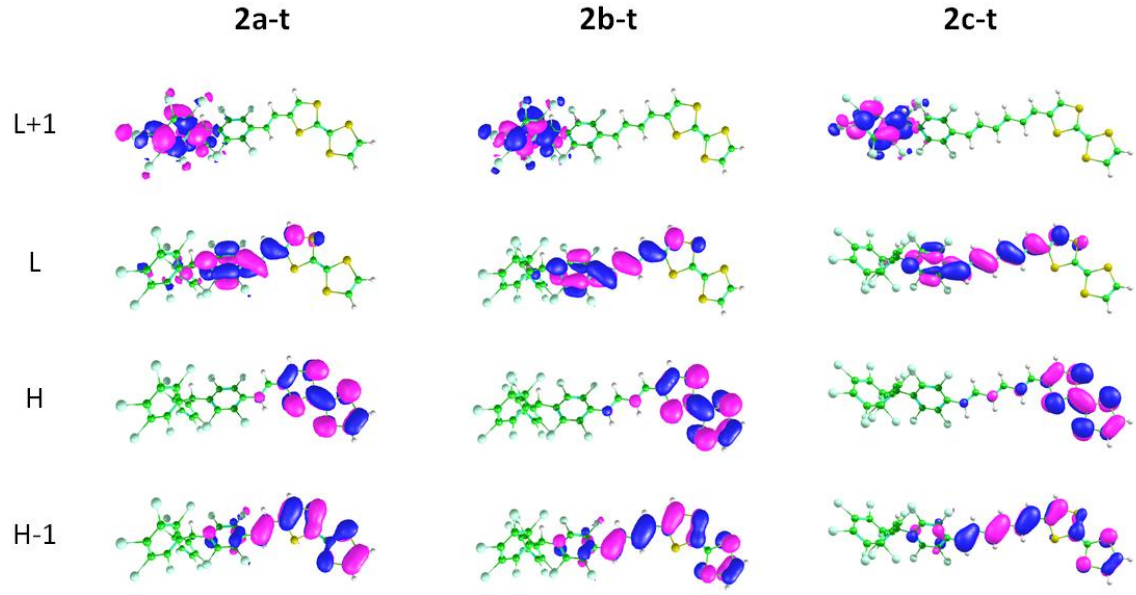

Figure S13. Frontier Molecular Orbitals for dyads **2a-2c**.

Frontier Molecular Orbitals of Open-Shell dyads 1a-1c (B3LYP/6-31G) (isovalue = 0.03)**

The HOMO is TTF-centered, as for the closed-shell systems. The SOMO (single occupied MO) is largely localized on the central carbon of the PT; unit. The α spin-orbital (SOMO) is lower in energy than the HOMO and its β partner corresponds to the lowest unoccupied β orbital (SUMO). For the β orbitals, the HOMO → SOMO gap is very small and will give rise to a low-energy charge-transfer electronic transition.

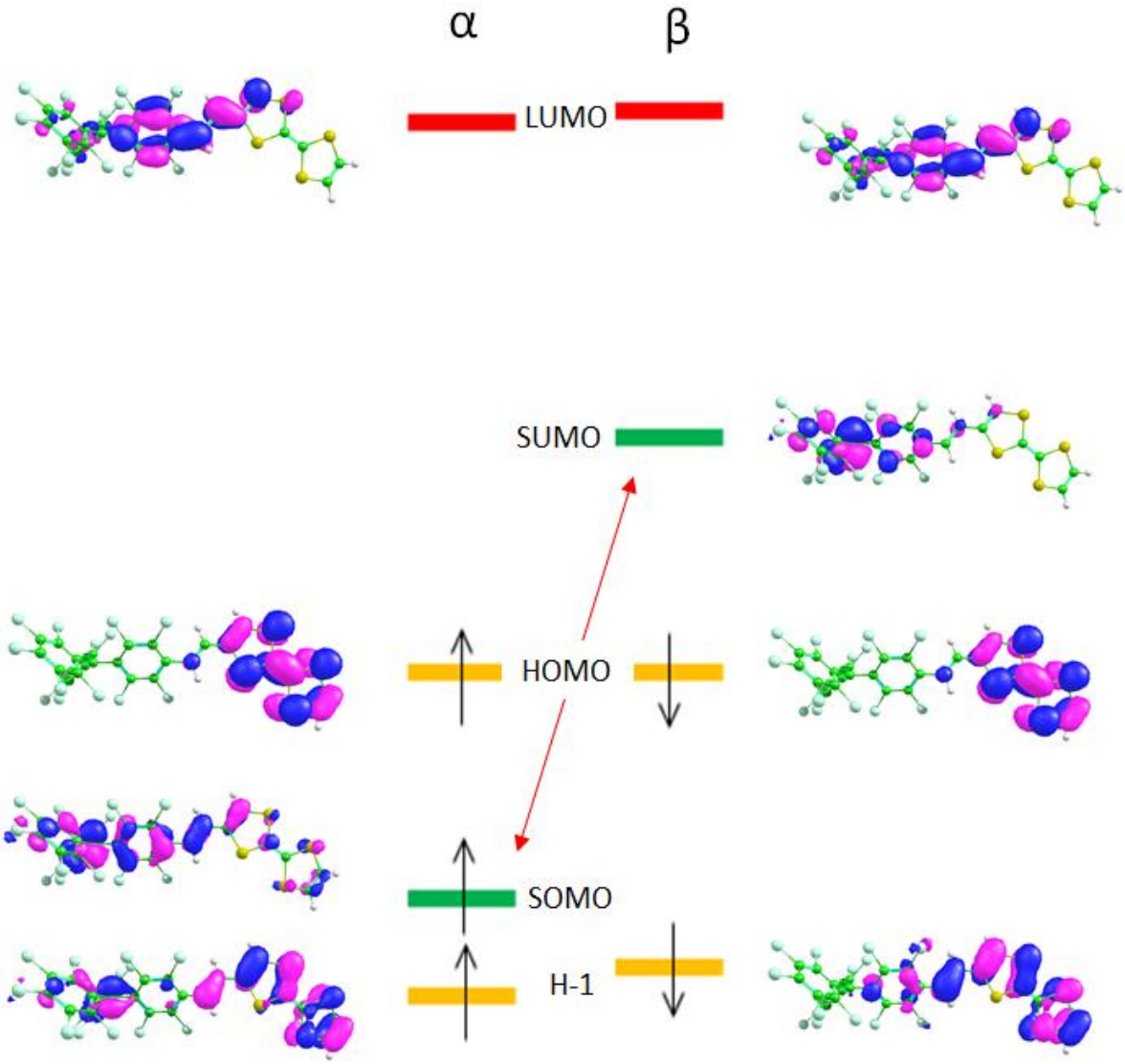

Figure S14. Frontier Molecular Orbitals for dyads **1a**.

Spin densities of Open-Shell dyads 1a-1c (B3LYP/6-31G) (isovalue = 0.001)**

The spin density calculated for the neutral species of the open-shell systems indicate that the unpaired electron is mainly located on the PTM unit. The spin density spreads over the bridge upon increasing the bridge length. Identical picture is obtained with the CAM-B3LYP results.

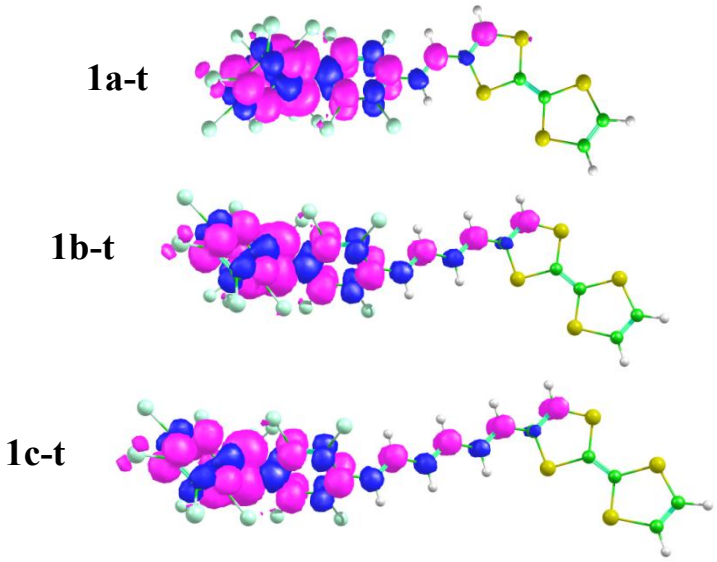

Figure S15. Spin densities of dyads **1a**.

Mulliken charges of dyads 1a-1c and 2a-2c (B3LYP/6-31G)**

A small electron density transfer (0.04–0.08 e) takes place in the ground state from the bridge and the TTF moiety to the ClTPM unit. The longer the bridge, the larger the electron density is going from the bridge to the ClTPM. The TTF unit is far from the acceptor ClTPM unit, and barely participates in the ground state electron transfer. However, comparing the s-cis and s-trans isomers, we find that the TTF in the more conjugated s-trans isomers donates more electron density to the ClTPM unit.

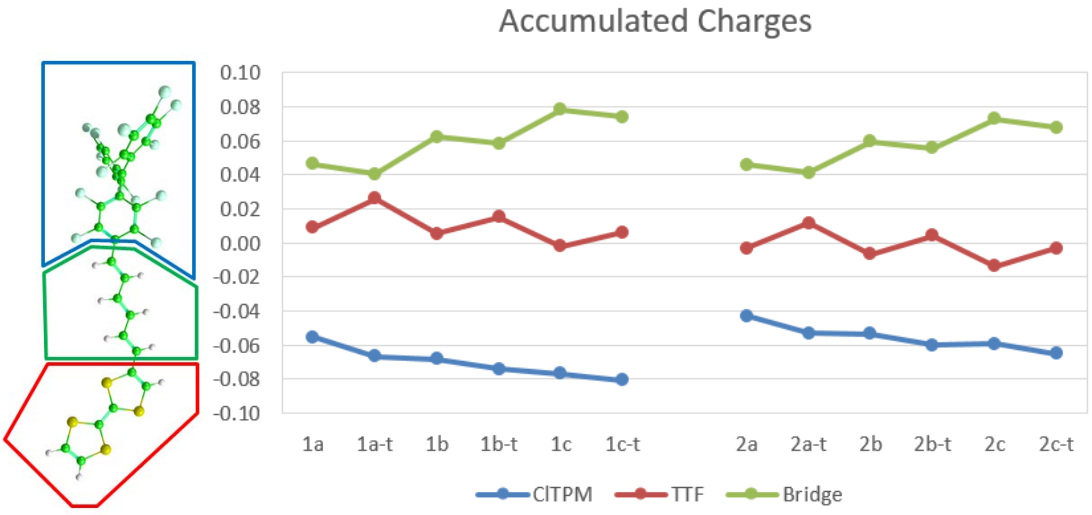

Figure S16. Mulliken charges of the different units for dyads **1a-1c** (*cis*- and *trans*-) and **2a-2c** (*cis*- and *trans*-).

Reduce/oxidized species: Spin density contours

Closed-shell systems (**2a-c**):
The reduction process to form the anion mainly takes place on the bridge as suggested by the LUMO topology. The first oxidation occurs on the TTF unit as expected by the HOMO shape. The second oxidation can take place on either the TTF or the PTM giving rise to a closed-shell singlet or to an open-shell triplet dication species, respectively (see the drawing for the dication).

Open-shell systems (**1a-c**):
Upon reduction, the extra electron enters the PTM unit (LUMO β or SUMO) generating a closed-shell anion. The first oxidation takes place on the TTF moiety and gives rise to a triplet cation species. The second oxidation occurs on the PTM fragment and the unpaired electron resides on the TTF. The third oxidation takes place on the TTF unit resulting in a closed-shell trication species.

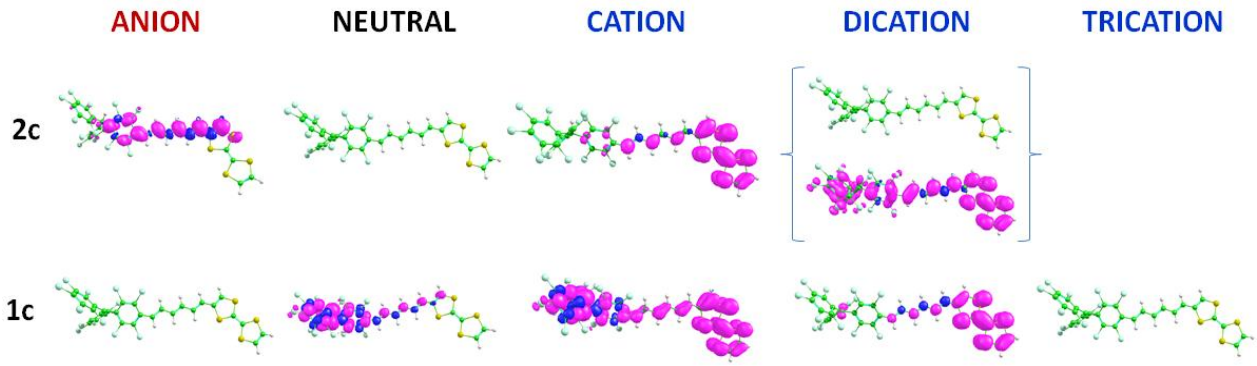

Figure S17. Spin density contours of the charged species derived from dyads **1a** and **2c**.

HOMO-LUMO gaps for dyads 1a-1c and 2a-2c

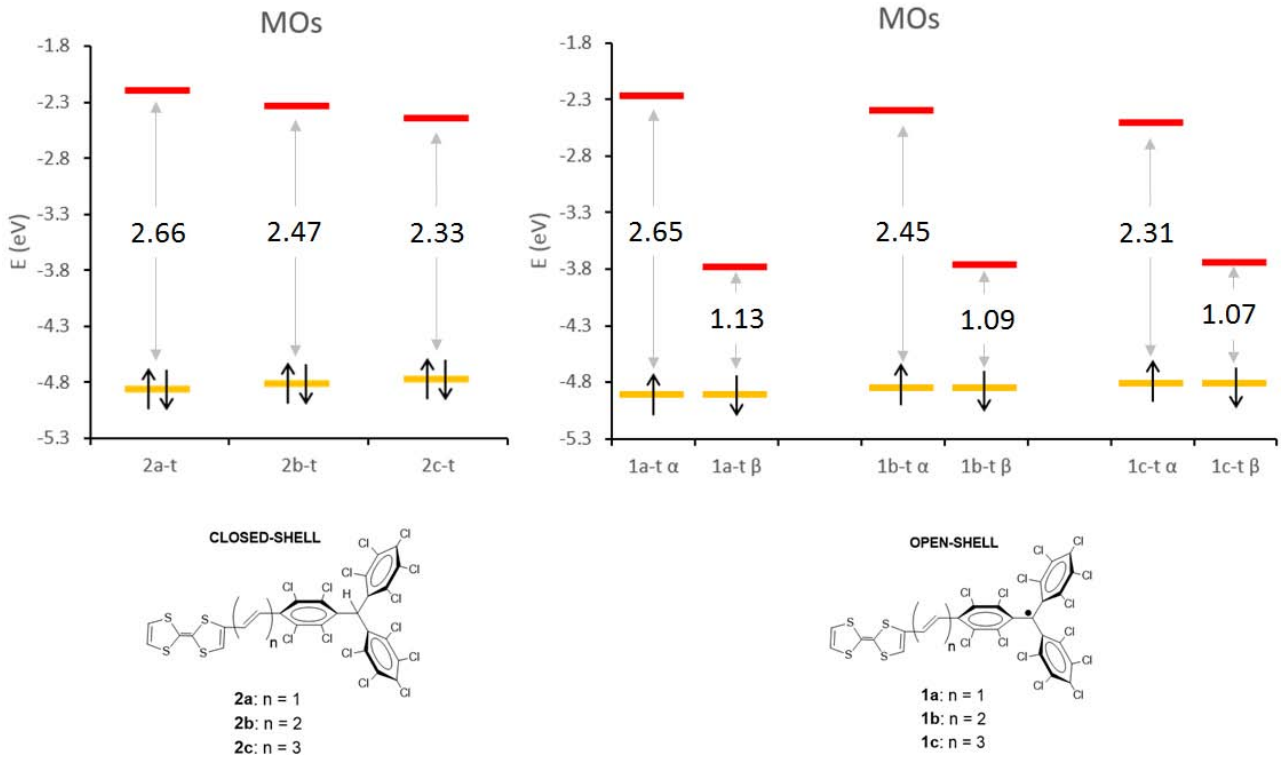

Figure S18. Orbital diagram indicating the energy difference between the HOMO and LUMO orbitals for dyads **1a-1c** and **2a-2c**.

Both theoretical HOMO-LUMO gaps and S_1 energies of dyads **2a-2c** show the same trend as obtained experimentally, with a reduction of the gap upon increasing the bridge length. For open-shell systems **1a-c**, theoretical HOMO-LUMO gaps are similar to the experimental ones. The lowest doublet excited states are computed a bit lower in energy due to the inherently underestimation of the charge-transfer excitations by the B3LYP functional. CAM-B3LYP gives too-high excited-state energies compared to B3LYP and experimental gaps.

HOMO-LUMO experimental gap:	HOMO-SUMO experimental gap:
2a: 2.20 eV	**1a**: 0.96 eV
2b: 2.15 eV	**1b**: 1.00 eV
2c: 2.10 eV	**1c**: 1.05 eV

Theoretical lowest singlet excited state S_1:	Theoretical lowest doublet excited state D_1:
2a-t: 2.25 eV	**1a-t**: 0.85 eV
2b-t: 2.11 eV	**1b-t**: 0.84 eV
2c-t: 2.01 eV	**1c-t**: 0.85 eV

Theoretical absorption spectra of dyads 1a-1c and 2a-2c

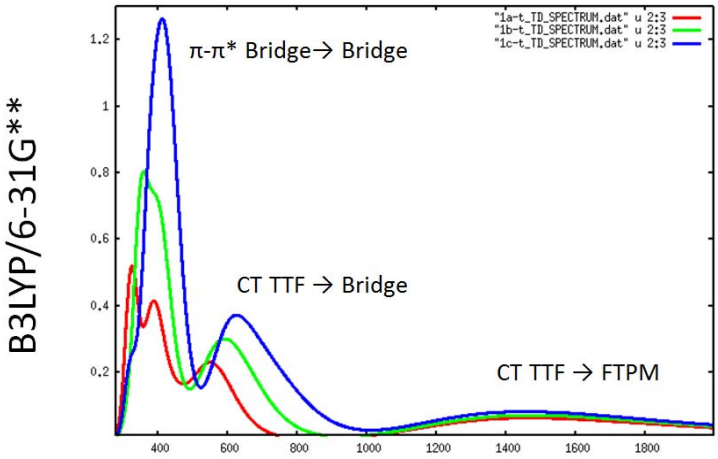

Figure S19. Theoretical absorption spectra of dyads **1a** (red line), **1b** (green line) and **1c** (blue line).

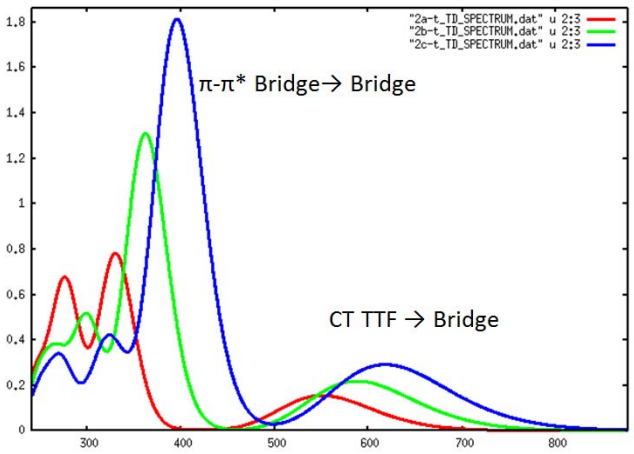

Figure S20. Theoretical absorption spectra of dyads **2a** (red line), **2b** (green line) and **2c** (blue line).

The theoretical absorption spectra computed at the B3LYP and CAM-B3LYP levels slightly differ due to the different amount of exact Hartree-Fock exchange. Both methods give the same qualitative description of the bands experimentally recorded in the 250-1000 range. We will use the B3LYP spectra presented in the previous slide although they underestimate the energy of charge-transfer bands.

For the open-shell systems, a weak low-lying charge-transfer transition is predicted around 1500 nm, which is assigned to the weak broad band experimentally observed around 900 nm. The transition corresponds to the D_1 state originating on the monoexcitation from the TTF (HOMO) to the ClTPM unit (SOMO). Two inner bands are predicted at 600 and 400 nm, which have a charge transfer (TTF → bridge) and a π-π* (bridge) nature, respectively. These two bands correspond to the transitions observed experimentally at 500 and 400 nm.

For the closed-shell systems, two main bands are computed in the 250-800 nm. The band calculated at 550-650 nm corresponds to the TTF → bridge (HOMO → LUMO) charge-transfer S_1 excitation and is assigned to the band experimentally observed at 450 nm. Otherwise, the band observed at 300-400 nm belongs to the π-π* electronic transition located in the bridge unit. Whereas the former does not suffer much displacement upon increasing the bridge length, the large blue-shift experienced by the π-π* band is nicely reproduced by the theoretical simulation.

Theoretical hyperpolarizabilities of dyads 1a-1c and 2a-2c (B3LYP/6-31G)**

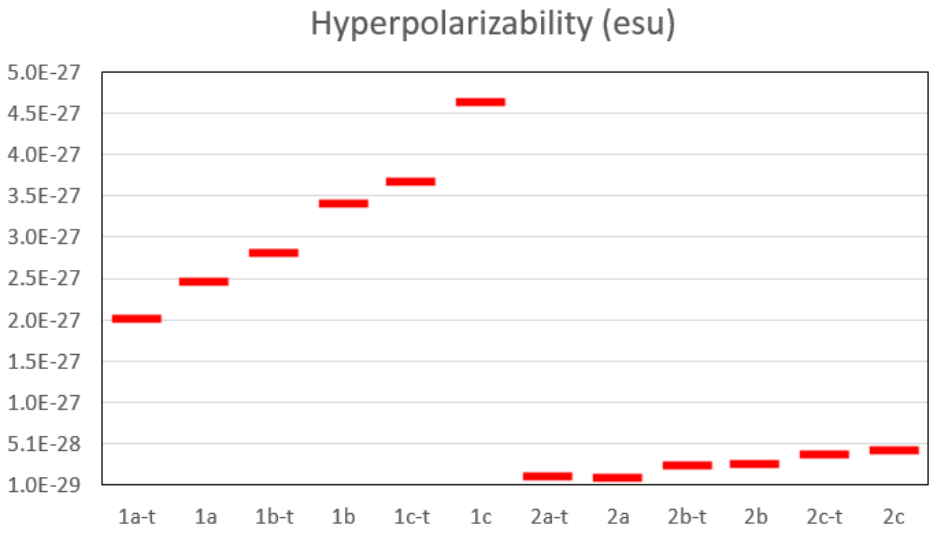

Figure S21. Absolute calculated values of β hyperpolarizabilities for dyads **1a-1c** (*cis* and *trans*) and for dyads **2a-2c** (*cis* and *trans*).

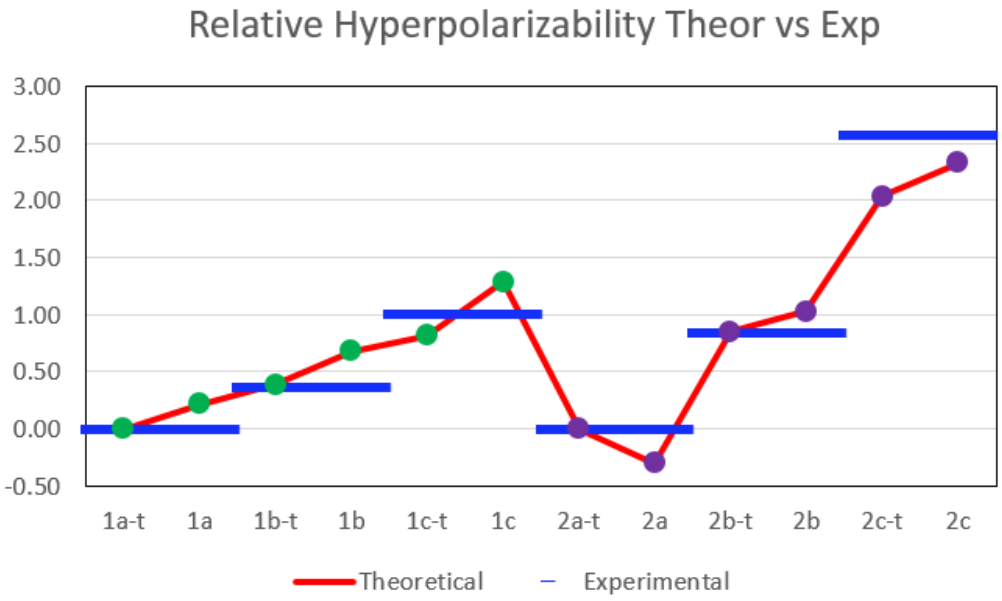

Figure S22. Comparison between relative experimental and theoretical values of β hyperpolarizabilities for dyads **1a-1c** (*cis* and *trans*) and for dyads **2a-2c** (*cis* and *trans*).